Pathogenesis of human mitochondrial diseases is modulated by reduced activity of the ubiquitin/proteasome system.

*Manuscript

Mitochondrial Stress Evokes Reduced Activity of the Ubiquitin/Proteasome-System Modulating Pathogenesis of Human Metabolic Diseases

Alexandra Segref[1], Éva Kevei[1], Wojciech Pokrzywa[1], Kathrin Schmeisser[2], Johannes Mansfeld[2,5], Nurit Livnat-Levanon[3], Regina Ensenauer[4], Michael H Glickman[3], Michael Ristow[2,5], and Thorsten Hoppe[1*]

[1]Institute for Genetics and Cologne Excellence Cluster on Cellular Stress Responses in Aging-Associated Diseases (CECAD), University of Cologne, Zülpicher Str. 47a, 50674 Cologne, Germany

[2]Department of Human Nutrition, Institute of Nutrition, University of Jena, 07743 Jena, Germany

[3]Department of Biology, Technion-Israel Institute of Technology, Haifa, Israel

[4]Research Center, Dr. von Hauner Children's Hospital, Ludwig-Maximilians-Universität München, 80337 Munich

[5]Energy Metabolism Laboratory, ETH Zürich, Schwerzenbach/Zürich, CH 8603, Switzerland

*Correspondence should be addressed to T.H.

*Correspondence: thorsten.hoppe@uni-koeln.de

Phone: +49 221 470 1503

Fax: +49 221 470 3402

Running title: Mitochondrial Stress Affects UPS Activity

Keywords: Mitochondria, ROS, *C. elegans*, UPS, Isovaleric acidemia

SUMMARY

Mitochondria maintain cellular homeostasis by coordinating ATP synthesis with metabolic activity, redox signaling, and apoptosis. Excessive levels of mitochondria-derived reactive oxygen species (ROS) promote mitochondrial dysfunction and human diseases including cancer, neurodegeneration, and numerous metabolic disorders. However, the molecular basis for the harmful effects of excessive ROS formation is largely unknown. Intriguingly, we identified a new link between mitochondrial stress and ubiquitin-dependent proteolysis supporting cellular surveillance both in *Caenorhabditis elegans* and humans. Worms defective in respiration with elevated ROS levels are limited in turnover of a GFP-based substrate protein, demonstrating that mitochondrial stress affects the ubiquitin/proteasome system (UPS). Moreover, we observed similar proteolytic defects for different human metabolic diseases caused by mitochondrial failure. Together, these results identify a conserved link between mitochondrial metabolism and ubiquitin-dependent proteostasis, suggesting that reduced UPS activity during pathological conditions might potentiate disease progression.

INTRODUCTION

In eukaryotic cells mitochondria are central for various cellular processes including the generation of energy and the orchestration of anabolic and catabolic metabolism. Defects in mitochondrial homeostasis are closely linked to the development of human pathologies such as cancer, neurodegenerative diseases, type 2 diabetes and additional metabolic disorders (Wallace, 2005). While limited

amounts of ROS appear to exert health-promoting functions in diverse species (Ristow and Zarse, 2010), mitochondrial dysfunction and protein damage are mainly caused by excessive formation of ROS, which are byproducts of oxidative phosphorylation and energy production in form of ATP (Livnat-Levanon and Glickman, 2010; Pagliarini et al., 2008; Tatsuta, 2009). Oxidative stress provoked by respiration defects usually results in misfolding and aggregation of mitochondrial proteins and finally leads to irreversible damage of mitochondria (Esposito et al., 1999; Tatsuta, 2009). Additionally, metabolic failure in catabolic pathways can cause accumulation of intermediates and biochemical stress within mitochondria (Sack and Finkel, 2012).

Several quality control mechanisms have evolved to maintain functional mitochondria by eliminating damaged proteins or even the entire organelle. Besides autophagic consumption of damaged mitochondria (called mitophagy), (Ashrafi and Schwarz, 2013; Kubli and Gustafsson, 2012) these mechanisms include different proteolytic quality control pathways in all mitochondrial compartments. One major system for protein degradation within mitochondria is based on the AAA-proteases Oma1 and Yme1, which mediate the turnover of inner mitochondrial membrane (IMM) proteins (Tatsuta, 2009; Tatsuta and Langer, 2009). The mitochondrial matrix harbors Lon and ClpP proteases, the latter is also discussed to be part of the mitochondrial unfolded protein response (UPR^{mt}) (Matsushima and Kaguni, 2012). In contrast, selective turnover of at least some outer mitochondrial membrane proteins involves the UPS (LivnatLevanon and Glickman, 2010). Damaged proteins are marked with a polyubiquitin chain formed by ubiquitin-activating enzymes (E1), ubiquitinconjugating enzymes (E2), and

ubiquitin protein ligases (E3) (Kerscher et al., 2006; Komander and Rape, 2012; Kuhlbrodt et al., 2005). In fact, the recently described mitochondria-associated degradation (MAD) pathway involves the ubiquitin-selective chaperone Cdc48/p97 in retrotranslocation of substrates from mitochondria for degradation by the 26S proteasome (Cohen et al., 2008; Franz et al., 2013; Heo et al., 2010; Karbowski and Youle, 2011; Taylor and Rutter, 2011). Upon high oxidative stress conditions, Cdc48 and UPS components including the E3 ligase HUWE1 are recruited to the mitochondrial outer membrane (Cohen et al., 2008; Heo et al., 2010; Taylor and Rutter, 2011). This network of different mitochondrial quality control systems is transcriptionally controlled by the UPR^{mt} (Haynes and Ron, 2010; Pellegrino et al., 2013; Zhao et al., 2002) however, the coordination between mitochondrial and cellular proteostasis pathways has not been addressed so far.

Here, we identified a novel link between mitochondrial metabolism and the UPS, which supports cellular surveillance. Inactivation of gene products engaged in oxidative phosphorylation or mitochondrial metabolism results in stabilization of a GFP-based substrate in the worm intestine, suggesting a yet unknown influence emanating from mitochondria on ubiquitin-dependent proteolysis in the cytosol. These defects in degradation are linked to enhanced oxidative stress since substrate stabilization can be suppressed by antioxidants. Moreover, an increase in ROS levels accumulating with acute depletion of mitochondrial gene transcripts strictly correlates with reduced UPS activity. The failure in ubiquitindependent proteolysis appears to be downstream of the ubiquitin conjugation process because increased proteasomal capacity is able to restore substrate turnover. Since we show similar results in patient cell lines defective in mitochondrial

metabolism, our findings support the idea that ROS-induced changes in ubiquitin-mediated proteolysis contribute to human mitochondrial pathology and might foster disease progression.

RESULTS

A Genetic Screen for Proteolytic Defects Identifies the E3 Ligase HECD-1 The UPS is central for the elimination of damaged proteins and the maintenance of cellular proteostasis; however, the physiological requirements for tissue function and organismal growth remained unclear. To identify new factors regulating protein turnover in multicellular organisms, we used a well established *in vivo* degradation assay that monitors even minor defects in proteostasis and stress response in *C. elegans* (Segref and Hoppe, 2012; Segref et al., 2011). This system is based on short-lived ubiquitin-fusion proteins (called UFD substrates), which was extensively applied to define fundamental mechanisms and important,

physiologically relevant degradation pathways of the UPS in single celled studies (Johnson et al., 1995; Koegl et al., 1999; Richly et al., 2005;

Seufert and Jentsch, 1992). Worms expressing a GFP-based UFD substrate UbV-GFP (Ub-GFP) under control of the ubiquitous *sur-5* promoter show no green fluorescence due to low steady state levels of the fusion protein enforced by polyubiquitylation of the N-terminal ubiquitin moiety and subsequent rapid proteasomal degradation. We used this reporter strain to monitor proteolytic defects in a forward genetic screen, where similar co-expression of the stable mCherry protein served as control to exclude transcriptional and translational changes (Figure 1A). 10 000 worms were mutagenized using ethyl methanesulfonate (EMS) and screened in the F2 generation for viable, GFPpositive mutants with increased Ub-GFP substrate levels (Figure 1A). Only nonlethal mutations were examined in our study, precluding disruption of essential functions such as proteasomal integrity. Among others, we first focused on four mutants with very strong and similar stabilization of GFP for further characterization (*hecd-1(hh2-4, hh9)*, Table S1). A non-complementation analysis revealed that these mutants were not able to complement each other (Table S2) and whole genome sequencing (WGS) of three mutants revealed independent stop mutations in the same gene called *hecd-1* (Supplemental Figure S1A). Additionally, a *hecd-1(tm2371)* deletion mutant caused Ub-GFP stabilization in all tissues, which confirmed the phenotype of the *hecd-1* mutants identified in our screen (Figures 1B and 1C). Moreover, these mutants did not complement the *hecd-1* deletion mutant (Table S2). Thus, our forward genetic screen identified HECD-1 as an important factor for ubiquitin-dependent substrate turnover. In fact,

HECD-1 is a HECT domain-containing E3 ligase related to human HECtD1 and HUWE1 (Leboucher et al., 2012; Shaye and Greenwald, 2011).

Loss of Functional IVD-1 and ACS-19 Limits Ubiquitin-dependent Protein Degradation

In addition, our screen identified two other mutants with strong stabilization of the Ub-GFP substrate, which are independent of *hecd-1* defects (*ivd-1(hh6), acs19(hh5),* Table S1, Table S2). SNP mapping and WGS placed the mutations into a 3.96 and 3.6 Mbp region on chromosomes III and IV, respectively (Supplemental Figures S1B and S1C). RNAi against potential candidates revealed that *ivd-1(RNAi)* and *acs-19(RNAi)* generate similar GFP stabilization in the intestine compared to the *ivd-1(hh6)* and *acs-19(hh5)* mutations found in the screen (Figure 2A-C). The mutation in *ivd-1(hh6)* causes a G to A splice donor mutation of the second intron, creating an aberrantly spliced mRNA (Supplemental Figure S1C). Consequently, sequencing of the *ivd-1(hh6)* cDNA confirmed a deletion of 45 nucleotides of the second exon, causing an in frame deletion of 15 amino acids that are highly conserved between different species including human IVD (Supplemental Figure S1D). In the *acs-19(hh5)* mutant the conserved glycine residue 311 (G311) is exchanged against arginine (R) (Supplemental Figures S1B and S1E). Thus, loss of important residues in the *ivd-1* or *acs-19* mutants together with the recessive nature in genetic complementation studies suggest reduced protein functions. Accordingly, transgenic expression of the respective wild-type genes could rescue the proteolytic defect of *ivd-1(hh6)* and *acs-19(hh5)* worms

(Figure 2D, Supplemental Figure S2A-C), indicating that IVD-1 and ACS-19 activity are linked to ubiquitindependent protein turnover.

IVD-1 is the orthologue of human isovaleryl-CoA dehydrogenase (IVD) (Mohsen et al., 2001), a mitochondrial enzyme with a defined role in the leucine catabolism pathway. During leucine degradation IVD catalyzes the conversion of isovaleryl-CoA into 3-methylcrotonyl-CoA (Supplemental Figure S2E) (Vockley and Ensenauer, 2006). We therefore asked if this particular step during leucine degradation might be important for turnover of the Ub-GFP substrate. RNAi against predicted orthologues genes of human *BCKDHB* and *MCCC1* expected to act upstream or downstream, respectively of *ivd-1* (Marcotte et al., 2000; Shaye and Greenwald, 2011), revealed an accumulation of Ub-GFP (Figure 2E, Supplemental Figure S2E), indicating that perturbance of the mitochondrial leucine degradation pathway *per se* affects ubiquitin-dependent protein turnover.

ACS-19 is defined as actetyl-CoA synthetase the predicted orthologue to human ACSS2, a cytosolic enzyme that catalyses the conversion of acetate to acetylCOA required for fatty acid cycle in the mitochondrial matrix (Shaye and Greenwald, 2011; Starai and Escalante-Semerena, 2004). In this regard it is interesting that the human HECT E3 ligase HUWE1 is also required for mitochondrial integrity because it targets mitofusin 2 for proteasomal degradation (Leboucher et al., 2012). Therefore, it is very likely that HECD-1 identified in our screen is also involved in mitochondrial maintenance in worms. These data indicate that our screen for UPS activity defects predominantly identified mutants with diminished mitochondrial function.

Increased Proteasomal Activity Restores Substrate Turnover in *ivd-1* and *acs-19* Mutants

To address the correlation between mitochondrial defects and decreased UPS activity we further evaluated the role of *ivd-1*, *acs-19*, and *hecd-1* in ubiquitindependent protein turnover. Importantly, RNAi-mediated depletion of *ivd-1*, *acs19*, and *hecd-1* had no effect on the amount of ^{K29,48R}Ub-GFP, a stable version of the substrate that cannot be polyubiquitylated, or of GFP alone (Supplemental Figure S2D). In contrast to loss of the E3 ligase HECD-1, the UFD substrate accumulates as polyubiquitylated forms in worms lacking IVD-1 or ACS-19 (Figure 2F). This comparison confirmed that the effects of *ivd-1*, *acs-19*, and *hecd-1* on steady state levels of Ub-GFP were due to diminished UPS function. In contrast to proteolysis of Ub-GFP in the cytosol, ER-associated protein degradation (ERAD) is not affected (Figure 3A). The ERAD substrate CPL^{W32A,Y35A} (Miedel et al., 2012) is only stabilized upon depletion of the Hrd3 ligase homolog *sel-1* (Grant and Greenwald, 1997), suggesting that IVD-1, ACS19, and HECD-1 do not participate in ERAD (Figure 3A). Indeed, the ERchaperone *hsp-4* was also not induced after *ivd-1*, *acs-19*, or *hecd-1* RNAi (Supplemental Figure S3A). The expression level of HSP-4 directly monitors defects in degradation of misfolded proteins accumulating in the ER lumen (Urano et al., 2002). It would thus appear that IVD-1, ACS-19 and HECD-1 are not relevant for ER function. To investigate whether the mutants have an overall defect in protein turnover, we analyzed the levels of polyubiquitylated substrates and found them to be unchanged compared to wild-type worms (Figure 3B). This is consistent with

the fact that these mutants are viable, whereas severe defects in the UPS induced by co-depletion of *cdc-48.1* and *cdc-48.2* lead to strong stabilization of polyubiquitylated substrates and lethality (Figure 3B) (Mouysset et al., 2008).

Since IVD-1, ACS-19, and HECD-1 seem to be linked to mitochondrial function, one explanation for the reduction in UPS activity could be a decrease in ATP production, which would affect E1-dependent ubiquitin activation and proteasomal degradation. However, measurement of the ATP levels in the *ivd-1*, *acs-19*, and *hecd-1* mutants revealed no decrease in the general ATP levels (Figure 3C). Thus, the defects in ubiquitin-dependent protein turnover are not due to changes in ATP availability. Similarly, the function of the 20S proteasome core particle is not reduced, as revealed by measurements of chymotrypsin-, trypsin-, and caspase-like activities (Figure 3D). We therefore examined if overexpression of the *rpn-6* subunit, a component of the 19S lid complex that was previously shown to increase assembly and activity of the 26S proteasome could suppress the degradation defects of our mutants (Vilchez et al., 2012a; Vilchez et al., 2012b). Interestingly, overexpression of *rpn-6* could indeed suppress the degradation defects of *ivd-1* and *acs-19* but not *hecd-1* RNAi depleted worms (Figure 3E). This is consistent with the proposed role of HECD-1 acting as an E3 ligase in substrate recognition and suggests that the defects seen upon *ivd-1* and *acs-19* inactivation occur downstream of substrate

recognition.

Enhanced Oxidative Stress Correlates with Impaired UPS Activity in Worms Lacking IVD-1, ACS-19, or HECD-1

To evaluate the induction of stress responses, we analyzed the levels of heat shock protein 70 (hsp70) homologs in the *ivd-1*, *acs-19*, and *hecd-1* mutants. Hsp-70 supports protein folding in the cytosol, whereas HSP-6 facilitates mitochondrial import, biogenesis, and energy generation (Kimura et al., 2007).

However, we could not detect any increase in cytosolic HSP-70 or mitochondrial HSP-6 levels (Supplemental Figure S3B and S3C). Therefore, we depleted key regulators of general stress pathways such as SKN-1, DAF-16, or HIF-1 by RNAi and examined proteolytic defects (Figure 4A) (An and Blackwell, 2003; Mehta et al., 2009; Ogg et al., 1997; Pickering et al., 2012). Interestingly, only down regulation of *skn-1* revealed a strong stabilization of the Ub-GFP substrate. Since SKN-1 is the major transcription factor acting upon oxidative stress (An and Blackwell, 2003; Pickering et al., 2012), we examined whether the oxidative stress response is induced in worms lacking IVD-1, ACS-19, and HECD-1. Indeed, *ivd-1*, *acs-19*, and *hecd-1* RNAi revealed an increase in the amount of the Glutathione S transferase GST-4, which expression is under tight control of

SKN-1 and thus reflecting enhanced oxidative stress (Figure 4B) (Kahn et al., 2008). Accordingly, acute depletion of *ivd-1* or *acs-19* by RNAi revealed a transient increase in ROS production (Figure 4C) whereas constitutive *ivd-1* and *acs-19* mutants exhibit reduced ROS levels in the steady-state (Supplemental Figure S3D). We reasoned that *ivd-1* and *acs-19* mutants might have adjusted to an initial accumulation of ROS due a process called mitohormesis, which was also reported for impaired insulin signaling by the DAF-2 receptor (Zarse et al., 2012). In further

support of an adaptive response mechanism, the *ivd-1* and *acs19* mutants exhibited reduced sensitivity upon treatment with antimycin A

(Supplemental Figure S3E), which is a drug known to increase mitochondrial ROS production (Chen et al., 2003; Turrens, 1997). Conversely, *hecd-1* mutant animals are more sensitive to antimycin A (Supplemental Figure S3E), consistent with the fact that worms lack a transient ROS increase after exposure to *hecd-1* RNAi (not shown) but mutant *hecd-1* rather show increased ROS levels in the steady-state (Supplemental Figure S3D). Importantly, the increased ROS level caused by *ivd-1* and *acs-19* depletion or antimycin A treatment can be efficiently reduced by addition of the antioxidant N-acetyl cysteine (NAC) (Figure 4D). Therefore, we wondered whether the observed changes in ROS strictly correlate with reduced UPS activity. Indeed, similar to the elevated ROS level NAC also attenuated the protein turnover defects in *ivd-1*, *acs-19*, and *hecd-1* mutants (Figure 4E), suggesting a general link between oxidative stress response in mitochondria and ubiquitin-dependent proteolysis in the cytosol.

Inhibition of Oxidative Phosphorylation Affects Ubiquitin-Dependent Degradation

Since our observations link ROS production with ubiquitin-dependent protein turnover defects, we next wondered whether mitochondrial dysfunction might be the underlying cause or contributes to this inhibition. Therefore we analyzed the stabilization of the Ub-GFP substrate upon RNAi depletion of critical components important for oxidative phosphorylation. Indeed, inhibition of respiratory chain

function by down regulation of complex I (*gas-1*, *nuo-1*, *nuo-6*), complex II (*mev1*), complex III (*isp-1*), and complex IV (*cco-1*) (Dingley et al., 2010; Shaye and Greenwald, 2011; Tsang et al., 2001) resulted in proteolytic failure in the cytosol (Figure 5A). Similarly, disruption of mitochondrial fission by *drp-1(RNAi)* (Labrousse et al., 1999) and mitochondrial UPR by *hsp-60(RNAi)* result in strong stabilization of the GFP-based reporter substrate (Figure 5A). In contrast, RNAi against *hsp-4* and *hsp-12.6*, major chaperons involved in ER stress and heat shock response, respectively, had no effect, which indicates a specific crosstalk between mitochondrial stress response and the UPS. As shown for *ivd-1* and *acs-19* depletion, the degradation defect of mitochondrial respiration mutants can be restored by *rpn-6* overexpression or NAC treatment (Figure 3E, 4E, 5B and C). Moreover, treatment with antimycin A and sodium azide, two drugs known to inhibit respiratory complex III and IV function of mitochondria (Chen et al., 1999; Rotsaert et al., 2008; Wilson and Erecinska, 1978), respectively, also resulted in strong stabilization of Ub-GFP (Figure 5D and E). In contrast, rotenone generating ROS at complex I exclusively in the mitochondrial matrix (Sena and Chandel, 2012) did not cause defects in UFD substrate degradation. Thus, oxidative and metabolic stress in mitochondria generally affect ubiquitindependent protein turnover in the cytosol.

Reduced UPS Activity Is Linked to Human Mitochondrial Disease Pathology

Our data strongly suggest that mitochondrial stress impairs UPS activity in *C. elegans*. Therefore, we asked whether this observation reflects a conserved link between mitochondrial metabolism and cellular ubiquitin-dependent proteostasis.

To address this question we used MelJuSo cell lines constitutively expressing the UFD or N-end rule substrate (Menendez-Benito et al., 2005). Whereas the Nterminal ubiquitin serves as degradation signal for the UFD substrate, deubiquitylation of N-end rule substrates defines the half-life of the remaining protein, which is related to the identity of its amino-terminal residue (Johnson et al., 1995; Varshavsky, 1992). As in worms, treatment with antimycin A resulted in strong stabilization of both ubiquitylated substrates (Figure 5D, E, Figure 6A, and Supplemental Figure S4A and S4B). In fact, this protein turnover defect can be restored by addition of NAC, indicating that it is based on increased ROS level (Figure 6B).

Since mutations in the *IVD* gene, encoding the human orthologue of IVD-1 in nematodes cause an autosomal recessive disorder called isovaleric acidemia (IVA), we were interested to study primary cells derived from IVA patients for defects in ubiquitin-dependent protein turnover. Fibroblasts from a patient with a severe phenotype (c.IVS4+2T>C) due to a homozygous splice site mutation (c.IVS4+2T>C/c.IVS4+2T>C) are lacking IVD protein completely, whereas an individual with a milder metabolic and clinical phenotype (c.932C>T) and homozygosity for a missense mutation (c.932C>T/c.932C>T) (Ensenauer et al., 2004) has normal IVD protein levels (Supplemental Figure S4C, Table S3). Western blot analysis of cell lysates showed that the overall polyubiquitin levels are unchanged in severe and mild IVA patient cells (Supplemental Figure S4D). Interestingly, transfection of the IVA fibroblasts with the N-end rule substrate revealed a strong stabilization of UbR-GFP especially in severe IVA patient cells (c.IVS4+2T>C) (Figure 6C). Moreover, the UFD substrate accumulated exclusively

in c.IVS4+2T>C fibroblasts as compared to control (c) or c.932C>T patient cells. The stabilization seen in fibroblasts with the severe IVA phenotype (c.IVS4+2T>C) is similar to treatment of control fibroblasts with the proteasomal inhibitor bortezomib (Figure 6D). These turnover defects correlate with increased ROS levels in the patient cells, with c.IVS4+2T>C exhibiting higher oxidative stress (Figure 6E). We tested whether the stabilization of the UFD and N-end rule substrate reflect defects in MAD. However, the levels of the OMM proteins mitofusin 2 (Mfn2) and Mcl1, important for mitochondrial fusion and apoptosis (Chan et al., 2011; Tanaka et al., 2010; Xu et al., 2011) did not increase in c.IVS4+2T>C patient cells (Figure 6F). Thus, in addition to the previously identified accumulation of metabolites (Table S3), patients suffering from IVA also display defects in ubiquitin-dependent protein turnover, which correlates with the degree of enzymatic impairment and disease pathology. Similarly, substrate degradation was reduced in cybrid cells from patients with a defect in the *COX1* gene affecting respiratory complex I (G6930A) (Bruno et al., 1999; King and Attardi, 1989) (Supplemental Figure S4E and S4F). Thus, it appears that comparable to *C. elegans*, mitochondrial dysfunction also affects UPS activity in humans.

Discussion

As defects in mitochondrial respiration are known to cause protein damage and mitochondrial dysfunction, the cytotoxic consequences of ROS remained enigmatic. With regard to human metabolic diseases it is particularly interesting how oxidative stress affects mitochondrial homeostasis and cellular protein quality control mechanisms. Here, we discovered a conserved influence of respiration defects and mitochondrial stress conditions on the efficiency of ubiquitin-dependent degradation pathways in the cytosol both in *C. elegans* and humans. Acute depletion of *ivd-1* and *acs-19* by RNAi caused a mild but significant increase in ROS, which correlates with defects in UFD substrate turnover. Whereas the ROS levels of the originally identified *ivd-1* and *acs-19* mutants are comparable to wild-type worms or even decreased, the mutants are still limited in substrate degradation. This discrepancy suggests that the adaptation against an initial increase in ROS is not able to restore protein turnover defects, probably by long term changes of respiratory and metabolic processes and might support the manifestation of chronic disorders (Figure 4C, D, Supplemental Figure S3D). Consequently, besides failure in leucine and fatty acid metabolism, down regulation of respiratory chain function, mitochondrial fission, or mitochondrial UPR demonstrated a general effect of oxidative and metabolic stress on ubiquitin-

dependent protein turnover both in *C. elegans* and human metabolic diseases (Figure 5A, D, E, and 6A, C, D, Supplemental Figure S4E,F).

Surprisingly, compared to the stabilization of UFD and N-end rule substrates, the turnover of mitochondrial proteins via the MAD pathway remained unchanged from a patient with severe IVA based on homozygosity for c.IVS4+2T>C (Figure 6C, D, F). Thus, in contrast to MAD, protein turnover in the cytosol is less efficient under mild oxidative stress conditions. Accordingly, ROSinduced degradation defects of *ivd-1* and *acs-19* or antimycin A-treated MelJuSo cells can be suppressed by the antioxidant NAC, which does not compensate for loss of the MAD regulator CDC-48 (Figure 4E, Figure 6B). Furthermore, *cdc48(RNAi)* aggravates the turnover defects of *ivd-1(hh6)* and *acs-19(hh5)* mutants thereby supporting the idea of differently affected proteolytic pathways (Supplemental Figure S5A and S5B). Defects in ubiquitin-dependent degradation caused by mitochondrial stress do not correlate with reduced viability of worm mutants. Conversely, the *acs-19* mutant exhibits increased lifespan compared to wild-type worms, which can be suppressed by NAC (Figure 7A, Supplemental Figure S5C). This observation suggests that beneficial consequences of mild oxidative stress are not overruled by limited UPS function (Figure 7A, Table S4). Loss of HECD-1 however results in constitutively increased ROS level (Supplemental Figure S3D), and reduced longevity which supports the idea that the HECT E3 ligase provides an overlapping function both in cytosolic and mitochondrial protein turnover related to the role of HUWE1 (Leboucher et al., 2012; Liu et al., 2011).

Conceptually, our work identified a new link between mitochondrial stress and UPS activity. This observation appears contradictory with regard to the inducible MAD pathway that degrades unfolded mitochondrial proteins in response to high oxidative and metabolic stress. However, specific reduction of prominent ubiquitin-mediated degradation pathways in the cytosol might further strengthen MAD by increasing the capacity of both conjugation and degradation processes at the mitochondrial outer membrane (Figure 7B). Indeed, overexpression of the 19S cap subunit *rpn-6* known to trigger both the integrity and activity of the 26S proteasome is able to compensate cytosolic ubiquitindependent turnover defects (Figure 3E) (Vilchez et al., 2012a; Vilchez et al., 2012b). Thus, it is intriguing to speculate that mild oxidative stress conditions reinforce MAD to maintain mitochondrial homeostasis and cellular surveillance.

Defects in mitochondrial metabolism are closely linked to chronic human diseases including cancer and neurodegeneration (Wallace, 2005). So far, changes in UPS function have not been specifically linked to mitochondrial diseases. Analyzing different human metabolic disorders, we noticed a strict correlation between mitochondrial failure and proteolytic defects similar to the observations in *C. elegans* (Figures 6C, D, Supplemental Figure S4E, F). According to our model the inhibition of cytosolic UPS pathways might contribute to survival on a cellular level, however, does not compensate the organismal consequences of the different mitochondrial defects (Figure 7B). In this regard, sustained maintenance of defective mitochondria could actually be the reason for disease pathology of otherwise harmful mutations. Patients with IVA specifically suffer from an accumulation of isovaleryl-CoA derivatives based on a defect in

isovaleryl-CoA dehydrogenase, resulting in acidification of blood and urine (Table S3). Early diagnosis combined with a protein restricted diet and medical therapy with isovaleryl-CoA conjugating agents can provide normal development even of severe cases (Vockley and Ensenauer, 2006). The accumulation of both UFD and N-end rule substrates is closely correlated with increased ROS level and the severity of the IVA disease pathology (Figure 6C, D, E). It is intriguing to speculate that changed UPS activity potentiates development and progression of metabolic diseases through a conserved mitochondrial surveillance response (MSR) (Figure 7B). Thus, the response mechanisms that limit ubiquitindependent protein turnover provide a new target for therapeutic intervention of chronic metabolic diseases caused by mitochondrial failure.

EXPERIMENTAL PROCEDURES

Strains

Worms were handled according to standard procedures and grown at 15°C or 20°C unless otherwise stated (Brenner, 1974). Mutations and transgenes used in this study are listed by chromosomes as follows: *cdc-48.1(tm544)II*, *unc119(ed4)III, sur-5::UbV-GFPIII, acs-19(tm4853)III, hecd-1(tm2371)IV, sur5::mCherry, sur-5::*^{K29,48R}*Ub-GFP, sur-5::GFP*. The Bristol strain N2 was used as wild-type and CB4856 Hawaii for mutant mapping studies. The strains AGD614 N2, *uthEx633 [Pmyo-3::GFP]* and AGD598 N2, *uthEx556 [Psur-5::rpn-6.1,Pmyo3::GFP]*, VK1879 *vkEx1879 [*P_{nhx-2}*cpl-1*^{W32AY35A}*::YFP;*P_{myo-2}*mCherry],* CL2166 *dvIs19 [pAF15(gst-4::GFP::NLS)]* , SJ4005 *zcIs4 [hsp-4::GFP]V*, SJ4100 *zcIs13[hsp-6::GFP]V* , BC10060 *dpy-5(e907); sEX884[hsp-70::GFP+pCeh361]*
were kind gifts from A. Dillin, C.J. Luke, C. Link, and D. Ron, respectively.

Mutagenesis

The strain PP608 *hhIs64 [unc-119(+); sur-5::UbV-GFP]III; hhIs73 [unc-119(+); sur-5::mCherry]* was grown at 15°C. 10 000 L4-staged hermaphrodites were treated with 50 mM EMS for 4 hr at room temperature. Worms were grown to day one of adulthood, bleached in sodium hypochloride solution and 86000 F1 worms obtained were cultured at 15°C until day one of adulthood. Worms were staged again by bleaching in sodium hypochlorite and the F2 population (16250 F2's) analyzed with a fluorescence stereomicroscope at day one and day two of adulthood for stabilized Ub-GFP signal. Mutant worms were selected to new plates

and cultured at 15°C. For further experiments *ivd-1(hh6)* and *acs-19(hh5)* were outcrossed six times against wild-type worms.

Mutant identification

Mutants obtained by EMS mutagenesis were analyzed for chromosome linkage (*ivd-1*, *acs-19* and *hecd-1*) and interval mapping (*ivd-1*, *acs-19*) according to Davis *et al*. (Davis et al., 2005). Here, mutant worms were crossed with CB4856 and Ub-GFP stabilization served as marker for the mutant phenotype. The mutants were sequenced by whole genome sequencing as described recently (Doitsidou et al., 2010; Sarin et al., 2008). For *acs-19* and *ivd-1* the mutations were verified after six times outcrossing against wild-type worms, selection of mutant phenotype and Sanger sequencing of the mutation.

RNAi

RNA interference was performed using the feeding method (Segref and Hoppe, 2012). Typically, worms were treated with RNAi from L1 stage and the phenotype observed during day one of adulthood unless otherwise stated. For *ivd-1*, *acs-19*, and *hecd-1* RNAi, stabilization of Ub-GFP served as an internal control for RNAi efficiency.

Generation of transgenic *C. elegans*

The original mutant strains obtained after EMS mutagenesis were injected with

10 ng/□L of the fosmids (WRM0620aH08 (for *acs-19*) or WRM061bH04 (for *ivd1*), and 100 ng/□L of pRF4 (*rol-6(su1006dm)*). Rescued F1 animals were analyzed at day one of adulthood for expression of GFP.

In vivo imaging

In vivo imaging was performed as described recently (Segref and Hoppe, 2012).

Immunoblotting

Worms were lyzed in SDS sample buffer and equal volumes applied to SDSPAGE as described recently (Segref and Hoppe, 2012). Western blotting was performed using antibodies against GFP (Clontech), ubiquitin (Upstate), mCherry (Abcam), tubulin (Sigma), and IVD (R. Ensenauer).

Polyubiquitylation

To investigate the polyubiquitylation status, worms were grown at 20°C till day one of adulthood. Worms were washed off the plates with 1x M9 buffer, settled on ice and the worm pellet lyzed in SDS sample buffer containing 10 mM NEM at 95°C for 4 minutes. Worms were analyzed by western blotting using an antibody against ubiquitin and tubulin as loading control. For polyubiquitylation of tissue culture cells, cells grown at similar densities were collected in SDS sample buffer and subjected to western blotting.

Quantification of ROS in Nematodes by MitoTracker Red Fluorescence

Nematodes were synchronized and either grown to day 1 adult stage or L1 larvae and treated with RNAi against, *ivd-1*, *acs-19*, or the empty control vector for 48 hrs. Worms were washed off the plates with S-basal buffer (pH 6) and allowed to settle by centrifugation (200 x g, 1 min). The worm pellet was transferred to plates spotted with 500 µl heat-inactivated OP50 (65°C, 30 min) mixed with 100 µl MitoTracker Red CM-H_2X stock solution (100 □M; freshly prepared) for 2 h at 20°C. To remove excess dye from the gut, the nematodes were washed with S-basal buffer 3 times and transferred to new plates with either OP50 or RNAi for 1 h at 20°C. 100 µl worm suspension aliquots in S-basal buffer were distributed into 8 wells/condition of a 96-well FLUOTRAC™ plate (Greiner Bio-One,). Fluorescence (ex: 570 nm, em: 610 nm) was measured in a plate reader (FLUOstar Optima, BMG Labtech,). To normalize the fluorescence signal, the protein content in the remaining worm suspension was determined using the Bradford assay.

Quantification of Hydrogen Peroxide Production of Nematodes by AmplexRed Fluorescence

Worms were treated with RNAi against *ivd-1*, *acs-19* or control vector with and without NAC (final 10 mM) for 48 h beginning at L1 stage. As internal positive control we incubated one part of the control worms on plates containing antimycin A (final 1 µM) for 2h right before the measurement. Worms were removed from plates with sodium-phosphate buffer (50 mM, pH 7.4) and washed twice. Ampliflu (Sigma-Aldrich) solution (final concentration 10 µM) and horseradish peroxidase (Sigma-Aldrich, final concentration 10 mU/ml) were added to the nematodes.

Measurement was carried out in 96-well Fluotrac plates (Bio Greiner One) using a micro plate reader (FLUOstar Optima, BMG Labtech) and filters for excitation at 544 nm and emission at 590 nm for 20 min at 20 °C.

Measurement of mitochondrial ROS in primary human fibroblasts

Primary human fibroblast cells were incubated with 5 □M MitoSOX Red (Molecular Probes®) for 30 minutes and ROS levels determined by imaging the cells with a Zeiss Meta 510 Confocal Laser Scanning Microscope (Abs.: 514 nm/Em.: 561 nm). Fluorescent images of MitoSOX-stained cells were taken with a 20x objective. Images were processed with ImageJ 1.48e software and mean fluorescence intensities of single cells are shown on the graph.

Stress tests

NGM plates containing 3 □□M rotenone (Sigma, 100 mM stock in DMSO), 2 □M antimycin A (Sigma,10 mM stock in 100% ethanol), or 0.2 mM sodium azide (Sigma, 200 mM stock in water, (only DMSO, ethanol or water was added to the respective control plates) were prepared freshly before the start of the experiment. The strain PP563 *hhIs64 [unc-119(+); sur-5::UbV-GFP]III* was grown from L4 stage for 12 h at 20°C and analyzed for expression of Ub-GFP by microscopy and western blotting. To analyze development, staged young adult worms were placed on NGM plates with ethanol as control or with 2 □M antimycin A and allowed to lay eggs for four hours. The adult worms were removed from the plates and the offspring grown at 15°C for 5 days. Worms were examined for their developmental

stage and grouped into adult worms or worms that had reached only a larval stage. For treatment with antioxidants, NGM plates containing N-acetyl cysteine (Sigma) (500 mM stock in water) were prepared freshly. L1-staged mutants worms expressing *sur-5::UbV-GFP* were added to the plates and grown at 15°C till day one of adulthood. Worms were collected in SDS sample buffer and analyzed by western blotting for expression of Ub-GFP.

ATP Measurements

200 day 1 adult hermaphrodite worms grown at 15°C were collected, washed 4 times in 1x M9 buffer, and frozen at -80°C before extract preparation. ATP levels were measured using the ATP bioluminescence kit HSII (Roche) according to the manufacturer's instruction. In brief, worms were lyzed in 500 □l lysis buffer provided with the kit, kept on ice for 10 min with brief vortexing every 2 min. The lysate was incubated at 95°C for 5 min, sonicated with a microsonicator and incubated at 95°C for 5 min. The lysates were centrifuged at 13000 rpm for 2 min at room temperature. 50 □l of the lysate was mixed with 50 □l of the Luminescence reagent provided with the kit using the Tecan infinite 200 microplate reader. Analysis was performed with a readout time of 10 s. An ATP curve in the extract was performed to ensure linearity of the measurement.

Proteasome activity

Proteasome activity was measured essentially as described previously (Vilchez et al., 2012b).

Lifespan analysis

Lifespan analysis was performed as described recently (Kuhlbrodt et al., 2011).

Cell culture and transfections

WT and G6930A cells were cultivated in DMEM with Glutamax supplemented with 5% FCS, 50 µg/ml Uridine, 1 mM sodium pyruvate, 100 µg/ml Streptomycin, and 100 U/ml Penicillin at 37°C and 5% CO2. Primary human *IVD* fibroblast cell lines were derived from skin of two children with isovaleric acidemia diagnosed by a disease-related metabolic pattern and homozygous *IVD* gene mutations, and of a healthy child undergoing inguinal hernia repair that served as a control cell line, after informed consent was obtained (Table S3). MelJuSo cells were cultivated in DMEM and fibroblasts in DMEM with Glutamax supplemented with 10% FCS, 100 µg/ml Streptomycin, and 100 U/ml Penicillin at 37°C and 5% CO2. Transfection was performed in 6 cm dishes using 10 µg of UbG76V-GFP or UbRGFP (Dantuma et al., 2000) obtained from N. Dantuma and 5 µg pmCherry-C1 with 10 µL Lipofectamine 2000 (Life Technologies) according to the manufacturers instruction. Cells were collected in SDS sample buffer after 24 h and analyzed by SDS-PAGE and western blotting. In case of Bortezomib treatment, 20 nM Bortezomib or as control DMSO was added to the culture 6 h after transfection.

Statistics

The mean +/- s.d. is reported unless otherwise indicated. Statistical comparisons among groups were determined using two-tailed Student's *t* test with a

significance value of $p \leq 0.05$.

ACKNOWLEDGMENTS

We thank S. Torres, G. Vopper, and S. Wullinger for technical support, M. Doitsidou, O. Hobert, and S. Motameny for advice on next generation sequencing analysis, A. Eck for advice on ATP measurements, and T. Wenz for comments on the manuscript. *C. elegans* strains were kindly provided by the *Caenorhabditis* Genetics Center (funded by the NIH Office of Research Infrastructure Programs (P40 OD010440), and the Mitani lab. We thank A. Fire, H. Kashkar, R. Wiesner, the Dana-Farber Cancer Institute and Geneservice Ltd for antibodies, plasmids, cDNAs, and patient cell lines. We particularly thank M.H. Glickman for exchange of unpublished results. This work is supported by grants of the Deutsche Forschungsgemeinschaft, especially the DIP8 grant
2014376 to M.H.G. and T.H., CECAD, and FOR885 to T.H., by the CoEN grant (an initiative of the DZNE, CIHR, and MRC) to T.H., by the German Federal Ministry of Education and Research (BMBF) grant 0315088 to R.E., and BMBF grant 0315581 for Systems Biology of Ageing (JenAge) to M.R.

AUTHOR CONTRIBUTIONS: A.S. and T.H. designed the study and analyzed data. A.S. contributed most of the results; E.K. analyzed mitochondrial stress response; W.P. performed turnover assays; E.K., J.M., K.S. and M.R. measured ROS; N.L.L. and M.H.G. provided advice and reagents; R.E. provided patient material; A.S. and T.H. wrote the manuscript. All authors discussed the results and commented on the manuscript.

COMPETING INTEREST

The authors declare that they have no competing financial interests.

REFERENCES

An, J.H., and Blackwell, T.K. (2003). SKN-1 links C. elegans mesendodermal specification to a conserved oxidative stress response. Genes Dev *17*, 1882-1893. Ashrafi, G., and Schwarz, T.L. (2013). The pathways of mitophagy for quality control and clearance of mitochondria. Cell Death Differ *20*, 31-42.

Brenner, S. (1974). The genetics of Caenorhabditis elegans. Genetics *77*, 71-94.

Bruno, C., Martinuzzi, A., Tang, Y., Andreu, A.L., Pallotti, F., Bonilla, E., Shanske, S., Fu, J., Sue, C.M., Angelini, C., *et al.* (1999). A stop-codon mutation in the human mtDNA cytochrome c oxidase I gene disrupts the functional structure of complex IV. Am J Hum Genet *65*, 611-620.

Chan, N.C., Salazar, A.M., Pham, A.H., Sweredoski, M.J., Kolawa, N.J., Graham, R.L., Hess, S., and Chan, D.C. (2011). Broad activation of the ubiquitin-proteasome system by Parkin is critical for mitophagy. Hum Mol Genet *20*, 1726-1737.
Chen, Q., Vazquez, E.J., Moghaddas, S., Hoppel, C.L., and Lesnefsky, E.J. (2003). Production of reactive oxygen species by mitochondria: central role of complex III. J Biol Chem *278*, 36027-36031.
Chen, Y.-R., Sturgeon, B.E., Gunther, M.R., and Mason, R.P. (1999). Electron Spin Resonance Investigation of the Cyanyl and Azidyl Radical Formation by Cytochrome c Oxidase. Journal of Biological Chemistry *274*, 24611-24616.
Cohen, M.M.J., Leboucher, G.P., Livnat-Levanon, N., Glickman, M.H., and Weissman, A.M. (2008). Ubiquitin-Proteasome-dependent Degradation of a Mitofusin, a Critical Regulator of Mitochondrial Fusion. Molecular Biology of the Cell *19*, 2457-2464.
Dantuma, N.P., Lindsten, K., Glas, R., Jellne, M., and Masucci, M.G. (2000). Short-lived green fluorescent proteins for quantifying ubiquitin/proteasome-dependent proteolysis in living cells. Nat Biotechnol *18*, 538-543.
Davis, M.W., Hammarlund, M., Harrach, T., Hullett, P., Olsen, S., and Jorgensen, E.M. (2005). Rapid single nucleotide polymorphism mapping in C. elegans. BMC Genomics *6*, 118.
Dingley, S., Polyak, E., Lightfoot, R., Ostrovsky, J., Rao, M., Greco, T., Ischiropoulos, H., and Falk, M.J. (2010). Mitochondrial respiratory chain dysfunction variably increases oxidant stress in Caenorhabditis elegans. Mitochondrion *10*, 125-136.
Doitsidou, M., Poole, R.J., Sarin, S., Bigelow, H., and Hobert, O. (2010). C. elegans mutant identification with a one-step whole-genome-sequencing and SNP mapping strategy. PLoS One *5*, e15435.
Ensenauer, R., Vockley, J., Willard, J.M., Huey, J.C., Sass, J.O., Edland, S.D., Burton, B.K., Berry, S.A., Santer, R., Grunert, S., *et al.* (2004). A common mutation is associated with a mild, potentially asymptomatic phenotype in patients with isovaleric acidemia diagnosed by newborn screening. Am J Hum Genet *75*, 1136-1142.
Esposito, L.A., Melov, S., Panov, A., Cottrell, B.A., and Wallace, D.C. (1999). Mitochondrial disease in mouse results in increased oxidative stress. Proc Natl Acad Sci U S A *96*, 4820-4825.
Franz, A., Ackermann, L., and Hoppe, T. (2013). Create and preserve: Proteostasis in development and aging is governed by Cdc48/p97/VCP. Biochim Biophys Acta. Grant, B., and Greenwald, I. (1997). Structure, function, and expression of SEL-1, a negative regulator of LIN-12 and GLP-1 in C. elegans. Development *124*, 637-644.
Haynes, C.M., and Ron, D. (2010). The mitochondrial UPR - protecting organelle protein homeostasis. J Cell Sci *123*, 3849-3855.
Heo, J.M., Livnat-Levanon, N., Taylor, E.B., Jones, K.T., Dephoure, N., Ring, J., Xie, J., Brodsky, J.L., Madeo, F., Gygi, S.P., *et al.* (2010). A stress-responsive system for mitochondrial protein degradation. Mol Cell *40*, 465-480.
Johnson, E.S., Ma, P.C., Ota, I.M., and Varshavsky, A. (1995). A proteolytic pathway that recognizes ubiquitin as a degradation signal. J Biol Chem *270*, 17442-17456. Kahn, N.W., Rea, S.L., Moyle, S., Kell, A., and Johnson, T.E. (2008). Proteasomal dysfunction activates the transcription factor SKN-1 and produces a selective oxidativestress response in Caenorhabditis elegans. Biochem J *409*, 205-213.

Karbowski, M., and Youle, R.J. (2011). Regulating mitochondrial outer membrane proteins by ubiquitination and proteasomal degradation. Curr Opin Cell Biol *23*, 476-482. Kerscher, O., Felberbaum, R., and Hochstrasser, M. (2006). Modification of proteins by ubiquitin and ubiquitin-like proteins. Annu Rev Cell Dev Biol *22*, 159-180.
Kimura, K., Tanaka, N., Nakamura, N., Takano, S., and Ohkuma, S. (2007). Knockdown of mitochondrial heat shock protein 70 promotes progeria-like phenotypes in caenorhabditis elegans. J Biol Chem *282*, 5910-5918.
King, M.P., and Attardi, G. (1989). Human cells lacking mtDNA: repopulation with exogenous mitochondria by complementation. Science *246*, 500-503.
Koegl, M., Hoppe, T., Schlenker, S., Ulrich, H.D., Mayer, T.U., and Jentsch, S. (1999). A novel ubiquitination factor, E4, is involved in multiubiquitin chain assembly. Cell *96*, 635-644.
Komander, D., and Rape, M. (2012). The ubiquitin code. Annu Rev Biochem *81*, 203229.
Kubli, D.A., and Gustafsson, A.B. (2012). Mitochondria and mitophagy: the yin and yang of cell death control. Circ Res *111*, 1208-1221.
Kuhlbrodt, K., Janiesch, P.C., Kevei, E., Segref, A., Barikbin, R., and Hoppe, T. (2011).
The Machado-Joseph disease deubiquitylase ATX-3 couples longevity and proteostasis. Nat Cell Biol *13*, 273-281.
Kuhlbrodt, K., Mouysset, J., and Hoppe, T. (2005). Orchestra for assembly and fate of polyubiquitin chains. Essays Biochem *41*, 1-14.
Labrousse, A.M., Zappaterra, M.D., Rube, D.A., and van der Bliek, A.M. (1999). C. elegans dynamin-related protein DRP-1 controls severing of the mitochondrial outer membrane. Mol Cell *4*, 815-826.
Leboucher, G.P., Tsai, Y.C., Yang, M., Shaw, K.C., Zhou, M., Veenstra, T.D., Glickman, M.H., and Weissman, A.M. (2012). Stress-induced phosphorylation and proteasomal degradation of mitofusin 2 facilitates mitochondrial fragmentation and apoptosis. Mol Cell *47*, 547-557.
Liu, G., Rogers, J., Murphy, C.T., and Rongo, C. (2011). EGF signalling activates the ubiquitin proteasome system to modulate C. elegans lifespan. EMBO J *30*, 2990-3003.
Livnat-Levanon, N., and Glickman, M.H. (2010). Ubiquitin-proteasome system and mitochondria - reciprocity. Biochim Biophys Acta *1809*, 80-87.
Marcotte, E.M., Xenarios, I., van Der Bliek, A.M., and Eisenberg, D. (2000). Localizing proteins in the cell from their phylogenetic profiles. Proc Natl Acad Sci U S A *97*, 1211512120.
Matsushima, Y., and Kaguni, L.S. (2012). Matrix proteases in mitochondrial DNA function. Biochimica et Biophysica Acta (BBA) - Gene Regulatory Mechanisms *1819*, 1080-1087.
Mehta, R., Steinkraus, K.A., Sutphin, G.L., Ramos, F.J., Shamieh, L.S., Huh, A., Davis, C., Chandler-Brown, D., and Kaeberlein, M. (2009). Proteasomal regulation of the hypoxic response modulates aging in C. elegans. Science *324*, 1196-1198.
Menendez-Benito, V., Verhoef, L.G., Masucci, M.G., and Dantuma, N.P. (2005). Endoplasmic reticulum stress compromises the ubiquitin-proteasome system. Hum Mol Genet *14*, 2787-2799.
Miedel, M.T., Graf, N.J., Stephen, K.E., Long, O.S., Pak, S.C., Perlmutter, D.H., Silverman, G.A., and Luke, C.J. (2012). A pro-cathepsin L mutant is a luminal substrate

for endoplasmic-reticulum-associated degradation in C. elegans. PLoS One *7*, e40145.
Mohsen, A.W., Navarette, B., and Vockley, J. (2001). Identification of Caenorhabditis elegans isovaleryl-CoA dehydrogenase and structural comparison with other acyl-CoA dehydrogenases. Mol Genet Metab *73*, 126-137.
Mouysset, J., Deichsel, A., Moser, S., Hoege, C., Hyman, A.A., Gartner, A., and Hoppe, T. (2008). Cell cycle progression requires the CDC-48UFD-1/NPL-4 complex for efficient DNA replication. Proc Natl Acad Sci U S A *105*, 12879-12884.
Ogg, S., Paradis, S., Gottlieb, S., Patterson, G.I., Lee, L., Tissenbaum, H.A., and Ruvkun, G. (1997). The Fork head transcription factor DAF-16 transduces insulin-like metabolic and longevity signals in C. elegans. Nature *389*, 994-999.
Pagliarini, D.J., Calvo, S.E., Chang, B., Sheth, S.A., Vafai, S.B., Ong, S.E., Walford, G.A., Sugiana, C., Boneh, A., Chen, W.K., *et al.* (2008). A mitochondrial protein compendium elucidates complex I disease biology. Cell *134*, 112-123.
Pellegrino, M.W., Nargund, A.M., and Haynes, C.M. (2013). Signaling the mitochondrial unfolded protein response. Biochim Biophys Acta *1833*, 410-416.
Pickering, A.M., Linder, R.A., Zhang, H., Forman, H.J., and Davies, K.J. (2012). Nrf2dependent induction of proteasome and Pa28alphabeta regulator are required for adaptation to oxidative stress. J Biol Chem *287*, 10021-10031.
Richly, H., Rape, M., Braun, S., Rumpf, S., Hoege, C., and Jentsch, S. (2005). A series of ubiquitin binding factors connects CDC48/p97 to substrate multiubiquitylation and proteasomal targeting. Cell *120*, 73-84.
Ristow, M., and Zarse, K. (2010). How increased oxidative stress promotes longevity and metabolic health: The concept of mitochondrial hormesis (mitohormesis). Exp Gerontol *45*, 410-418.
Rotsaert, F.A.J., Ding, M.G., and Trumpower, B.L. (2008). Differential efficacy of inhibition of mitochondrial and bacterial cytochrome bc1 complexes by center N inhibitors antimycin, ilicicolin H and funiculosin. Biochimica et Biophysica Acta (BBA) - Bioenergetics *1777*, 211-219.
Sack, M.N., and Finkel, T. (2012). Mitochondrial metabolism, sirtuins, and aging. Cold Spring Harb Perspect Biol *4*.
Sarin, S., Prabhu, S., O'Meara, M.M., Pe'er, I., and Hobert, O. (2008). Caenorhabditis elegans mutant allele identification by whole-genome sequencing. Nat Methods *5*, 865867.
Segref, A., and Hoppe, T. (2012). Analysis of ubiquitin-dependent proteolysis in Caenorhabditis elegans. Methods Mol Biol *832*, 531-544.
Segref, A., Torres, S., and Hoppe, T. (2011). A screenable in vivo assay to study proteostasis networks in Caenorhabditis elegans. Genetics *187*, 1235-1240.
Sena, L.A., and Chandel, N.S. (2012). Physiological roles of mitochondrial reactive oxygen species. Mol Cell *48*, 158-167.
Seufert, W., and Jentsch, S. (1992). In vivo function of the proteasome in the ubiquitin pathway. EMBO J *11*, 3077-3080.
Shaye, D.D., and Greenwald, I. (2011). OrthoList: A Compendium of C. elegans Genes with Human Orthologs. PLoS One *6*, e20085.
Starai, V.J., and Escalante-Semerena, J.C. (2004). Acetyl-coenzyme A synthetase (AMP forming). Cell Mol Life Sci *61*, 2020-2030.

Tanaka, A., Cleland, M.M., Xu, S., Narendra, D.P., Suen, D.F., Karbowski, M., and Youle, R.J. (2010). Proteasome and p97 mediate mitophagy and degradation of mitofusins induced by Parkin. J Cell Biol *191*, 1367-1380.
Tatsuta, T. (2009). Protein quality control in mitochondria. J Biochem *146*, 455-461.
Tatsuta, T., and Langer, T. (2009). AAA proteases in mitochondria: diverse functions of membrane-bound proteolytic machines. Res Microbiol *160*, 711-717.
Taylor, E.B., and Rutter, J. (2011). Mitochondrial quality control by the ubiquitinproteasome system. Biochem Soc Trans *39*, 1509-1513.
Tsang, W.Y., Sayles, L.C., Grad, L.I., Pilgrim, D.B., and Lemire, B.D. (2001). Mitochondrial respiratory chain deficiency in Caenorhabditis elegans results in developmental arrest and increased life span. J Biol Chem *276*, 32240-32246.
Turrens, J.F. (1997). Superoxide production by the mitochondrial respiratory chain. Biosci Rep *17*, 3-8.
Urano, F., Calfon, M., Yoneda, T., Yun, C., Kiraly, M., Clark, S.G., and Ron, D. (2002). A survival pathway for Caenorhabditis elegans with a blocked unfolded protein response. J Cell Biol *158*, 639-646.
Varshavsky, A. (1992). The N-end rule. Cell *69*, 725-735.
Vilchez, D., Boyer, L., Morantte, I., Lutz, M., Merkwirth, C., Joyce, D., Spencer, B., Page, L., Masliah, E., Berggren, W.T., *et al.* (2012a). Increased proteasome activity in human embryonic stem cells is regulated by PSMD11. Nature *489*, 304-308.
Vilchez, D., Morantte, I., Liu, Z., Douglas, P.M., Merkwirth, C., Rodrigues, A.P., Manning, G., and Dillin, A. (2012b). RPN-6 determines C. elegans longevity under proteotoxic stress conditions. Nature *489*, 263-268.
Vockley, J., and Ensenauer, R. (2006). Isovaleric acidemia: new aspects of genetic and phenotypic heterogeneity. Am J Med Genet C Semin Med Genet *142C*, 95-103. Wallace, D.C. (2005). A mitochondrial paradigm of metabolic and degenerative diseases, aging, and cancer: a dawn for evolutionary medicine. Annu Rev Genet *39*, 359-407. Wilson, D.F., and Erecinska, M. (1978). Ligands of cytochrome c oxidase. Methods Enzymol *53*, 191-197.
Xu, S., Peng, G., Wang, Y., Fang, S., and Karbowski, M. (2011). The AAA-ATPase p97 is essential for outer mitochondrial membrane protein turnover. Mol Biol Cell *22*, 291300.
Zarse, K., Schmeisser, S., Groth, M., Priebe, S., Beuster, G., Kuhlow, D., Guthke, R., Platzer, M., Kahn, C.R., and Ristow, M. (2012). Impaired insulin/IGF1 signaling extends life span by promoting mitochondrial L-proline catabolism to induce a transient ROS signal. Cell Metab *15*, 451-465.
Zhao, Q., Wang, J., Levichkin, I.V., Stasinopoulos, S., Ryan, M.T., and Hoogenraad, N.J. (2002). A mitochondrial specific stress response in mammalian cells. EMBO J *21*, 44114419.

FIGURE LEGENDS

Figure 1. A mutagenesis screen to identify novel genes involved in UPS-mediated protein turnover.

A) Outline of the mutagenesis screen performed on hermaphrodite worms expressing the UPS reporter *Psur-5::UbV-GFP*. B) Fluorescence and Nomarski images of worms expressing Ub-GFP in wild-type (WT) or *hecd-1* mutant worms as indicated. Scale bar: 100 □m. C) Protein lysates of worms displayed in (B), including one additional allele *hecd-1(hh9),* were analyzed by SDS-PAGE and immunoblotting against GFP and tubulin as loading control.

Figure 2. Novel mutations in *ivd-1* and *acs-19* display defects in Ub-GFP turnover.

A) Fluorescence and Nomarski images of wild-type (WT) or *ivd-1(hh6)* mutant worms and of wild-type worms grown on *control (RNAi)* (*ctrl (RNAi)*) or *ivd-1(RNAi)* plates analyzed for stabilization of Ub-GFP at day 1 of adulthood. Scale bar: 100 □m. B) As in (A) but *acs-19(hh5)* worms were compared to WT and *acs-19(RNAi)*. Scale bar: 100 □m. C) Western blot analysis of protein lysates derived from day 1 adult worms expressing Ub-GFP as indicated. The blot was probed against GFP and tubulin as loading control. D) Fluorescence and Nomarski images of worms expressing Ub-GFP in *ivd-1(hh6)* mutants with or without the *ivd-1* gene-containing fosmid WRM061bH04 (*ivd1(hh6)+ivd-1*). Bottom: *acs-19(hh5)* mutants without (*acs-19(hh5*)) or with the *acs-19* gene-containing fosmid WRM0620aH08 (*acs-19(hh5)+ acs-19*). Fluorescent images were taken with the same exposure times. Scale bars: 100 □m. E) Lysates of day 1 adult worms expressing Ub-GFP treated with RNAi against the *C. elegans* orthologues of human branched chain

keto acid dehydrogenase E1 (*tag-173*) and alpha methylcrotonyl coenzyme A carboxylase 1 (*mccc-1*) involved in leucine catabolism were analyzed by western blotting against GFP and tubulin. F) Worms expressing Ub-GFP were depleted by RNAi for the indicated genes and analyzed by western blotting as in (C).

Figure 3. Protein turnover in *ivd-1*, *acs-19*, or *hecd-1 worms*.

A) Worms expressing either CPL-1$^{W32A,\ Y35A}$-YFP (CPL-1$^{W32A,\ Y35A}$) or Ub-GFP (UbVGFP) were RNAi-treated as indicated and lysates of worms analyzed by western blotting with an antibody against GFP that also recognizes YFP (anti-GFP) and tubulin. B) Lysates of day 1 adult mutant worms were analyzed for the presence of polyubiquitylated substrates by western blotting against polyubiquitin. As a control *cdc48.1(tm544)* mutants were either treated with *control (RNAi)* or *cdc-48.2 (RNAi)*. C) Relative ATP levels in day 1 old wild-type (WT) and mutant worms. Results display three (*ivd-1*, *hecd-1*), five (WT) and four independent experiments (*acs-19*), average +/- s.d. ** $p \leq 0.01$. D) Relative slopes of chymotrypsin, trypsin, and caspase-like proteasomal activity of day 1 old wild-type (WT) and mutant worms. Averages are displayed of 5 to 7 independent experiments +/- s.e.m, $p>0.05$. E) Hermaphrodites expressing either GFP (*GFP(OE))* or *rpn-6.1* and *GFP* (*rpn-6.1,GFP(OE)*) on extrachromosomal arrays and integrated *sur-5::UbV-GFP* were RNAi-treated and lysates examined by western blotting as in (2C).

Figure 4. Cellular stress response by disruption of *ivd-1*, *acs-19*, or *hecd-1* function.

A) Hermaphrodites expressing *sur-5::UbV-GFP* or *sur-5::GFP* were RNAi-treated against the indicated genes and lysates of day 1 adult worms subjected to western blotting against GFP and tubulin. B) Hermaphrodites were RNAi-treated against the indicated genes and analyzed for the expression of *gst-4::GFP* at day 1 adult stage. Western blotting was performed as in (2C). C) ROS levels of WT hermaphrodites (expressing *sur-5::UbV-GFP* as control for RNAi efficiency) that were treated with the indicated RNAi's for 48 h (control, *acs-19*, *ivd-1*). Data are averages derived from 2 independent experiments +/- s.e.m, ***p ≤ 0.001. D) H_2O_2 production measured by Amplex Red staining of the strain used in (C) treated with RNAi as indicated or antimycin A with or without N-acetyl cysteine (NAC). Averages from 2 independent experiments +/- s.e.m., p values: *** p ≤ 0.001, * p ≤ 0.05, (-) NAC compared to the control, (+) NAC were compared to the (–) NAC counterpart to indicate significant suppression by NAC. E) Mutant worms expressing *sur-5::UbV-GFP* were grown on control plates (c), or plates containing 10 mM NAC from L1 stage to day 1 of adulthood. Western blotting was performed as in (2C), short exp., long exp: short and long exposure of the blot, respectively.

Figure 5. Disruption of mitochondrial function impairs Ub-GFP turnover.

A) Wild-type worms expressing *sur-5::UbV-GFP* were treated with the indicated RNAi's and lysates of worms examined by western blotting as in (2C). B) Hermaphrodites expressing either GFP (-) (*GFP(OE))* or *rpn-6.1* and *GFP* (+) (*rpn-6.1,GFP(OE))* on extrachromosomal arrays and integrated *sur-5::UbV-GFP* were RNAi-treated and lysates examined by western blotting as in (2C). C) Wild-type worms expressing *sur5::UbV-GFP* were treated with the indicated RNAi's from L1 to adulthood and moved to control (-) or 10 mM NAC-containing NGM plates (+) 24 hr prior to collection. Lysates of worms were

examined by western blotting as in (2C). D) Fluorescence and Nomarski images of wild-type worms expressing Ub-GFP either untreated (control), or treated with

3 □□M rotenone, 2□□M antimycin A, or 0.2 mM sodium azide (NaN3) for 12 h. Scale bar: 1 mm. (E) Lysates of worms displayed in (D) were analyzed by western blotting against GFP and tubulin.

Figure 6. Disease-related mitochondrial mutations disrupt UPS-mediated protein turnover in humans.

A) MelJuSo cell lines stably expressing UbR-YFP or UbG76V-YFP were pre-treated for 18 hours with ethanol as control (-) or 100 □M antimycin A (in ethanol) followed by 100 □g/ml cycloheximide for the indicated time points. Cell lysates were analyzed by western blotting against YFP and tubulin. B) Cell lines from (A) were pretreated with H_2O (-) or the indicated concentrations of N-acetylcysteine (NAC), followed by 18 hrs incubation with 100 □M antimycin A with or without NAC. Cell lysates were analyzed as in (A). C, D) Primary human control fibroblasts (c) and fibroblasts from IVD-deficient patients with a severe (c.IVS4+2T>C) or mild (c.932C>T) phenotype were transfected with UbR-GFP or UbG76V-GFP and mCherry as transfection control and cell lysates were analyzed by western blotting against GFP, mCherry and tubulin. E) Mitochondrial

ROS content was measured in fibroblast cells described in (C) using MitoSOX staining. Mean fluorescence intensities normalized to the average fluorescence measured in the control cell line are shown with the s.e.m. (c: 1.00 +/- 0.04; c.IVS4+2T>C: 1.59 +/- 0.06 (***$p \leq 0.001$); c.932C>T: 1.16 +/- 0.06 (*$p \leq 0.05$)); (n_c = 166; $n_{c.IVS4+2T>C}$ = 139; $n_{c.932C>T}$ = 132). F) Untransfected fibroblast cell lines as described in (C) were analyzed by western blotting with antibodies against Mfn2, Mcl1, and tubulin.

Figure 7. ROS-induced attenuation of ubiquitin-dependent proteolysis in the cytosol supports cellular surveillance.

A) Lifespan analysis of worms as indicated grown at 20°C on NGM containing OP50. Detailed statistics are provided in Table S4. B) Damaged mitochondrial proteins accumulating upon high ROS levels are degraded via the recently identified MAD pathway. This process involves the stress induced recruitment of the ubiquitin-selective chaperone Cdc48 to the outer mitochondrial membrane, which facilitates the retrotranslocation and targeting of mitochondrial proteins to the UPS machinery. In contrast, low levels of ROS reduce the activity of cytosolic protein degradation pathways (UFD and N-end rule pathway), which might further strengthen MAD by increasing the capacity of both conjugation and degradation processes at the mitochondrial outer membrane. Thus, the general effect of low oxidative stress on the UPS reflects a conserved mitochondrial surveillance response (MSR).

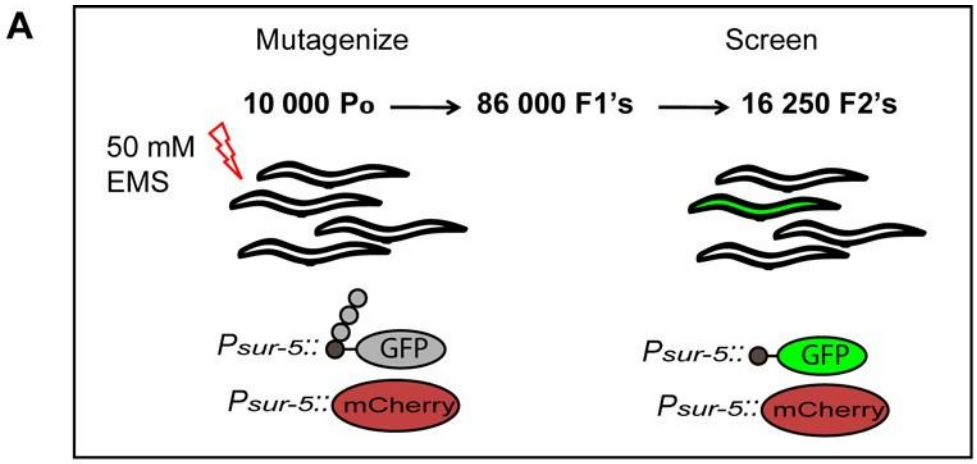
A
Mutagenize
Screen
10 000 Po
86 000 F1's
16 250 F2's
50 mM
EMS
Psur-5::
GFP
Psur-5::
mCherry
Psur-5::
GFP
Psur-5::
mCherry

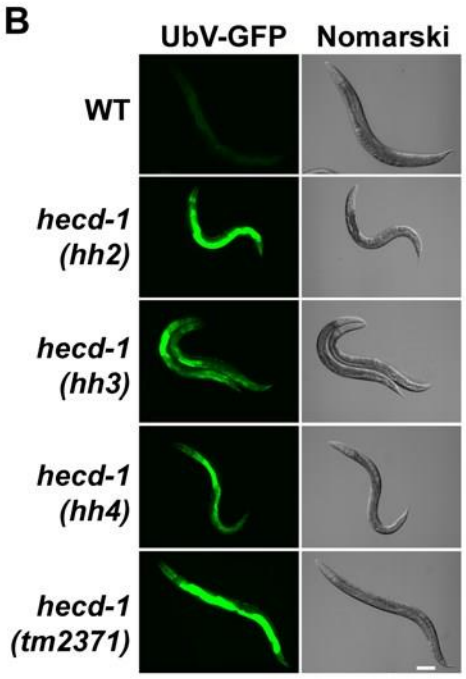
B
UbV-GFP
Nomarski
WT
hecd-1
(hh2)
hecd-1
(hh3)
hecd-1
(hh4)
hecd-1
(tm2371)

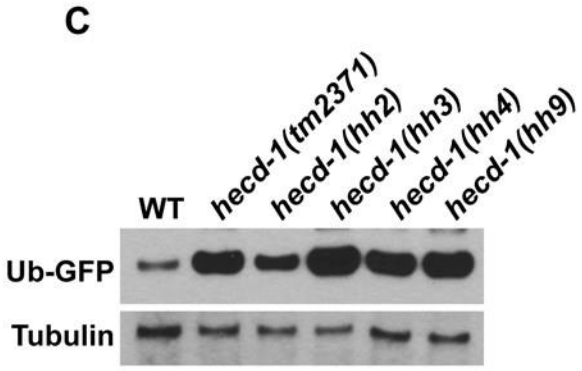
C
WT
hecd-1(tm2371)
hecd-1(hh2)
hecd-1(hh3)
hecd-1(hh4)
hecd-1(hh9)
Ub-GFP
Tubulin

Figure 1

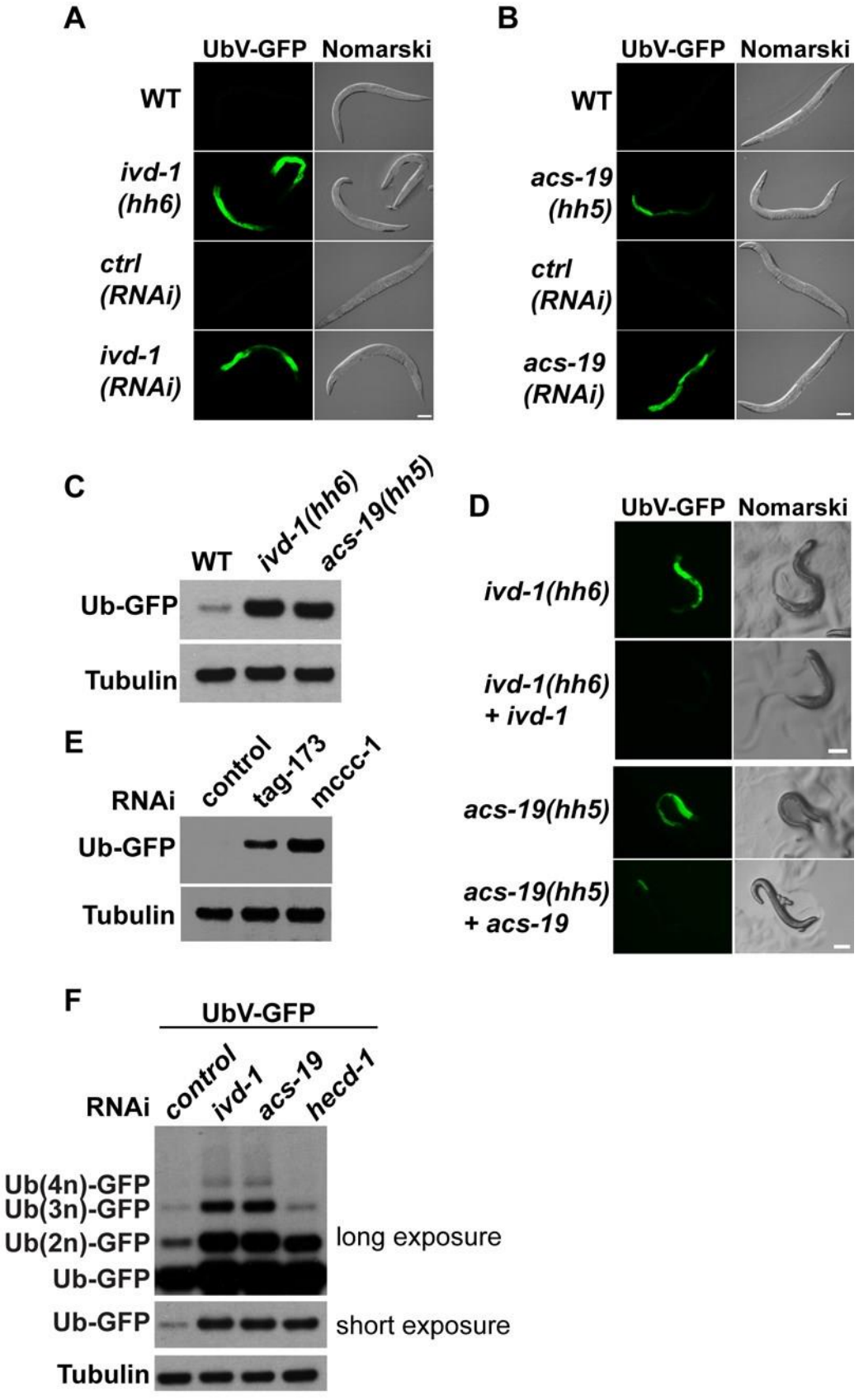
A
UbV-GFP
Nomarski
WT
ivd-1 (hh6)
ctrl (RNAi)
ivd-1 (RNAi)
B
UbV-GFP
Nomarski
WT
acs-19 (hh5)
ctrl (RNAi)
acs-19 (RNAi)
C
WT
ivd-1(hh6)
acs-19(hh5)
Ub-GFP
Tubulin
D
UbV-GFP
Nomarski
ivd-1(hh6)
ivd-1(hh6) + ivd-1
acs-19(hh5)
acs-19(hh5) + acs-19
E
RNAi
control
tag-173
mccc-1
Ub-GFP
Tubulin
F
UbV-GFP
RNAi
control
ivd-1
acs-19
hecd-1
Ub(4n)-GFP
Ub(3n)-GFP
Ub(2n)-GFP
Ub-GFP
long exposure
Ub-GFP
short exposure
Tubulin

Figure 2

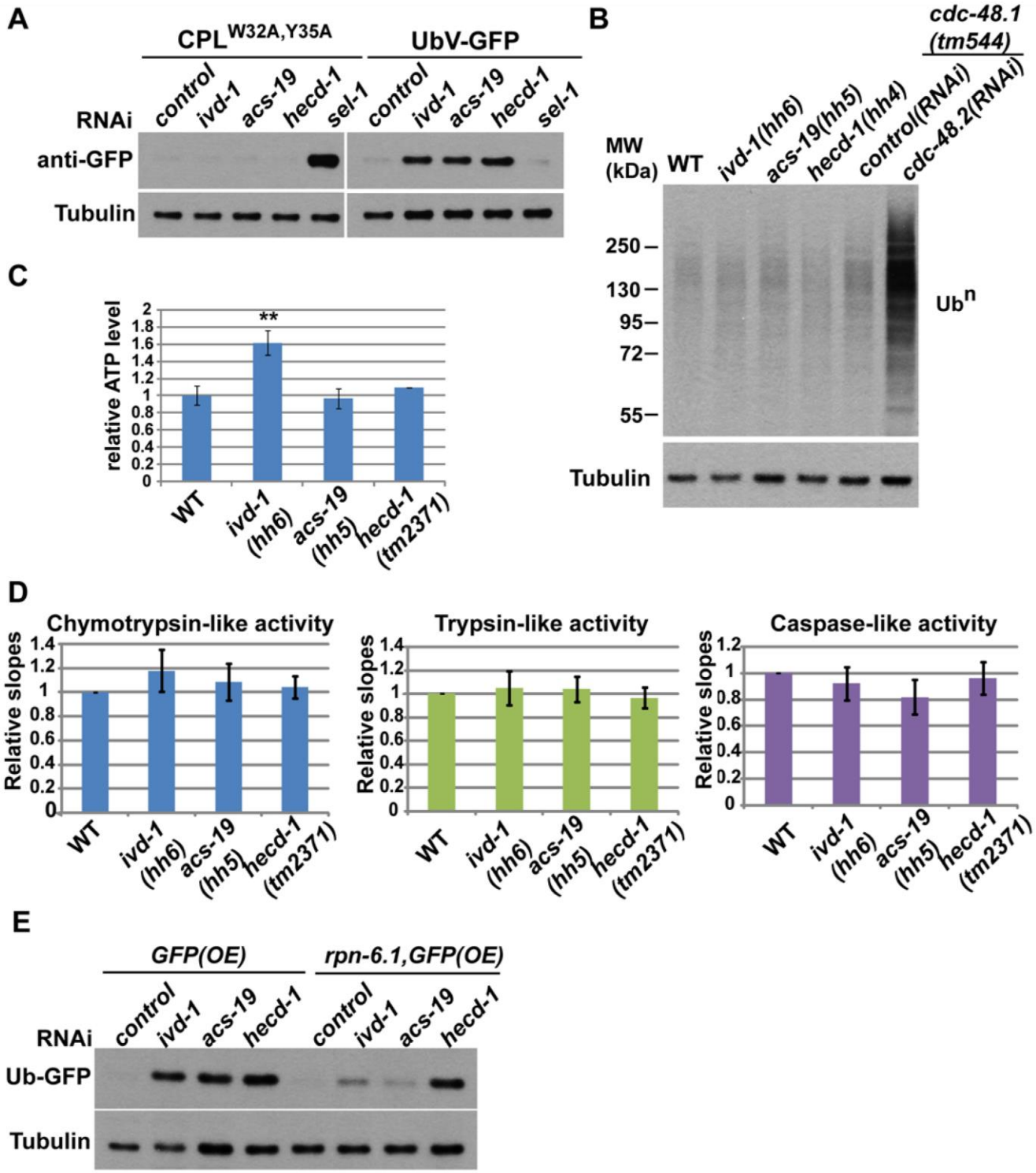
A
CPL W32A,Y35A
UbV-GFP
RNAi
control
ivd-1
acs-19
hecd-1
sel-1
anti-GFP
Tubulin
B
cdc-48.1 (tm544)
MW (kDa)
WT
ivd-1(hh6)
acs-19(hh5)
hecd-1(hh4)
control(RNAi)
cdc-48.2(RNAi)
250
130
95
72
55
Ub^n
Tubulin
C
relative ATP level
**
WT
ivd-1 (hh6)
acs-19 (hh5)
hecd-1 (tm2371)
D
Chymotrypsin-like activity
Trypsin-like activity
Caspase-like activity
Relative slopes
E
GFP(OE)
rpn-6.1,GFP(OE)
Ub-GFP
Tubulin

Figure 3

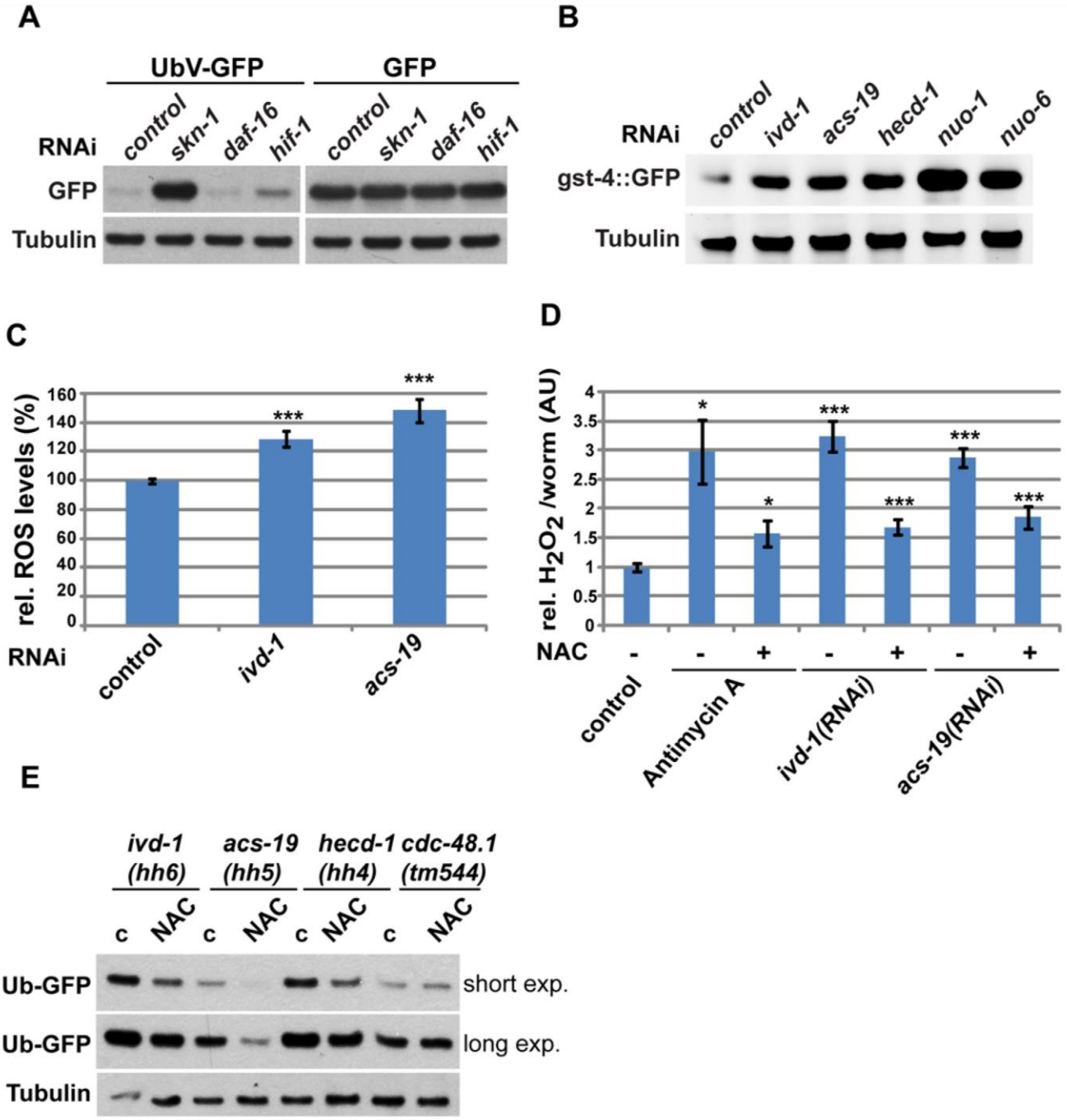
A
UbV-GFP
GFP
RNAi
control
skn-1
daf-16
hif-1
GFP
Tubulin
B
RNAi
control
ivd-1
acs-19
hecd-1
nuo-1
nuo-6
gst-4::GFP
Tubulin
C
rel. ROS levels (%)
RNAi
control
ivd-1
acs-19
D
rel. H2O2 /worm (AU)
NAC
control
Antimycin A
ivd-1(RNAi)
acs-19(RNAi)
E
ivd-1 (hh6)
acs-19 (hh5)
hecd-1 (hh4)
cdc-48.1 (tm544)
c
NAC
Ub-GFP
short exp.
Ub-GFP
long exp.
Tubulin

Figure 4

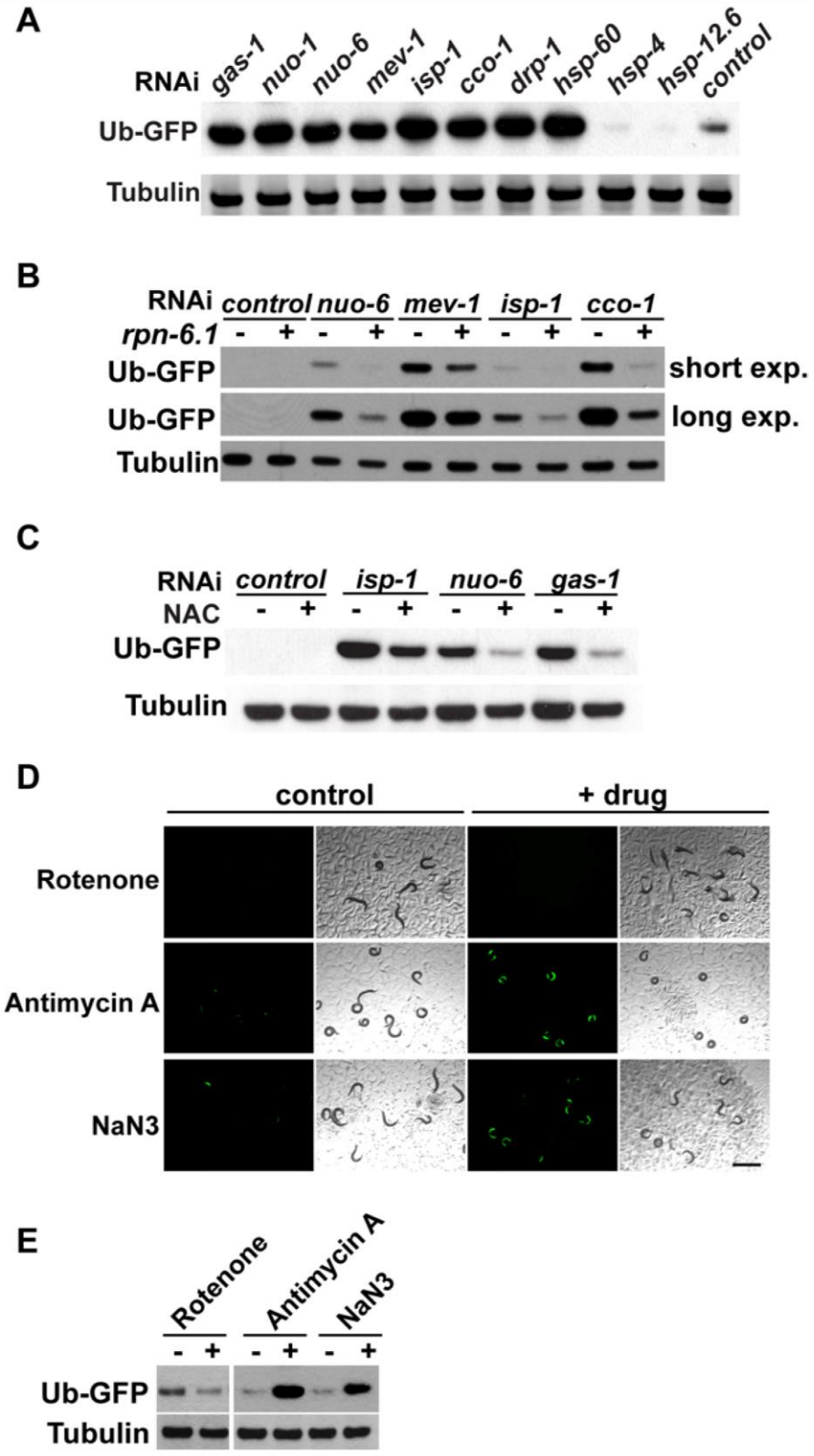
A
RNAi
gas-1
nuo-1
nuo-6
mev-1
isp-1
cco-1
drp-1
hsp-60
hsp-4
hsp-12.6
control
Ub-GFP
Tubulin
B
RNAi
control
nuo-6
mev-1
isp-1
cco-1
rpn-6.1
- + - + - + - + - +
Ub-GFP
short exp.
Ub-GFP
long exp.
Tubulin
C
RNAi
control
isp-1
nuo-6
gas-1
NAC
- + - + - + - +
Ub-GFP
Tubulin
D
control
+ drug
Rotenone
Antimycin A
NaN3
E
Rotenone
Antimycin A
NaN3
- + - + - +
Ub-GFP
Tubulin

Figure 5

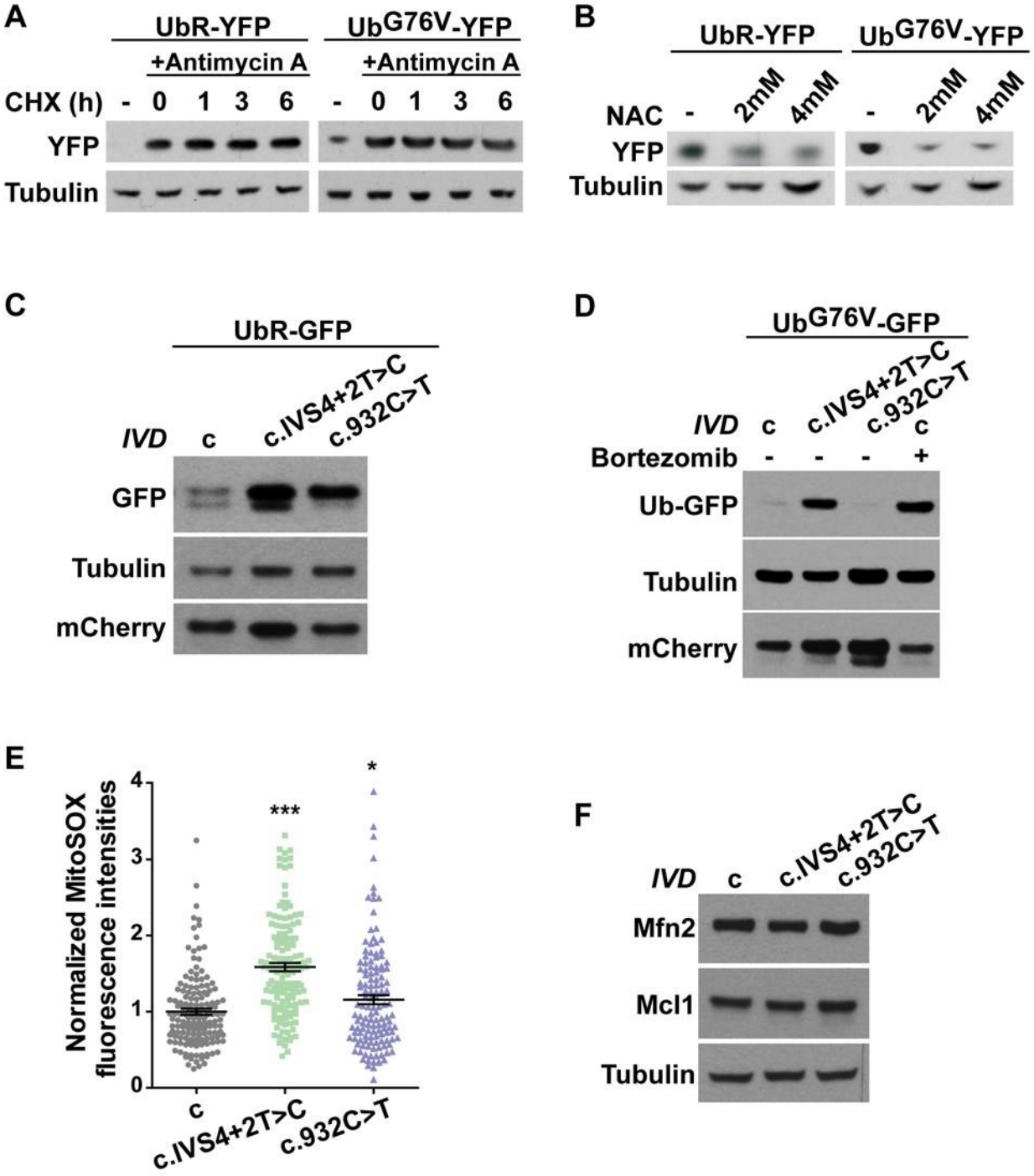
A
UbR-YFP
UbG76V-YFP
+Antimycin A
+Antimycin A
CHX (h) - 0 1 3 6 - 0 1 3 6
YFP
Tubulin
B
UbR-YFP
UbG76V-YFP
NAC - 2mM 4mM - 2mM 4mM
YFP
Tubulin
C
UbR-GFP
IVD c c.IVS4+2T>C c.932C>T
GFP
Tubulin
mCherry
D
UbG76V-GFP
IVD c c.IVS4+2T>C c.932C>T c
Bortezomib - - - +
Ub-GFP
Tubulin
mCherry
E
Normalized MitoSOX fluorescence intensities
0
1
2
3
4
***
*
c
c.IVS4+2T>C
c.932C>T
F
IVD c c.IVS4+2T>C c.932C>T
Mfn2
Mcl1
Tubulin

Figure 6

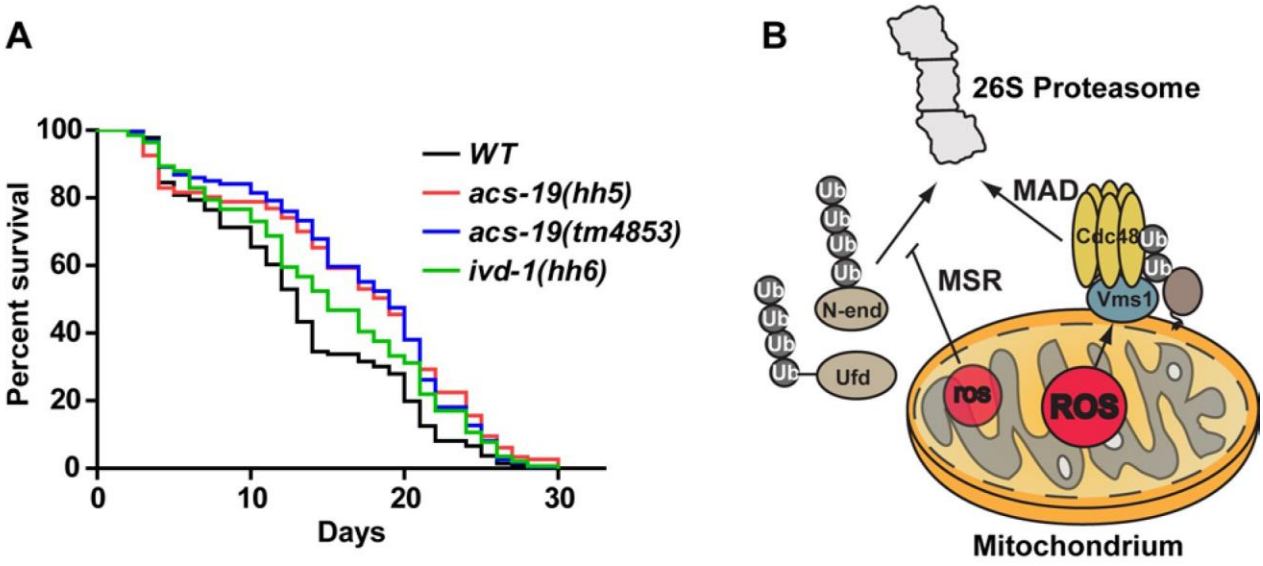
A
Percent survival
100
80
60
40
20
0
0
10
20
30
Days
WT
acs-19(hh5)
acs-19(tm4853)
ivd-1(hh6)
B
26S Proteasome
MAD
Cdc48
Ub
Vms1
MSR
N-end
Ufd
ros
ROS
Mitochondrium

Figure 7

Inventory of Supplemental Information

Supplemental Inventory

Supplemental Figure 1 linked to main Figure 1 and 2 (genetic identification of the mutations, multiple sequence alignment of the identified *acs-19* and *ivd-1* mutations)

Supplemental Figure 2 linked to Figure 2 (genetic rescue of *ivd-1* and *acs-19*, leucine catabolism analysis)

Supplemental Figure 3 linked to Figure 4 and 5 (analysis of different stress pathways, ROS levels)

Supplemental Figure 4 linked to Figure 6 (analysis of MelJuso and patient cells)

Supplemental Figure 5 *cdc-48(RNAi)* and Lifespan linked to Figure 7

Supplemental Figure legends 1-5

Supplemental Table 1 linked to Figure 1A (phenotypes of mutants identified in the EMS screen)

Supplemental Table 2 linked to Figure 1 and 2 (genetic complementation studies of the mutants identified in the screen)

Supplemental Table 3 linked to Figure 6 (explanation of human *Ivd* mutations and phenotype)

Supplemental Table 4 linked to Figure 7A (statistics of lifespan data)

Supplemental Table 5 linked to Supplemental Figure 5 (statistics of lifespan analysis)

Supplemental Figure Legends

Supplemental Figure Legends

Supplemental Figure 1

Schematic outline of the *hecd-1*, *acs-19* and *ivd-1* mutations identified. A) Outline of the identified *hecd-1(hh2) –(hh4)* alleles as resolved by whole genome sequencing. B) Using SNP analysis, the *acs-19* mutation was mapped to a 3.96 Mbp region between the SNPs CE3-127 (physical location 3359035) and snp_F56C9 (physical location 7320107) (Davis et al., 2005) on chromosome III. C) The *ivd-1* mutation was mapped to a 3.6 Mbp region between the SNPs pKP4064 (physical location 4285309) and pKP4077 (physical location 7900254) on chromosome IV. D) *C. elegans* IVD-1 (AAD21088.1) was aligned with *Drosophila* CG6638-PA (AAF50398.1), *Homo sapiens* IVD (AAA52711.1) and *Arabidopsis* IVD (AEE78020.1) using the Clustal W2 multiple sequence alignment program and further processed using the Jalview multiple alignment editor. In brackets are the GenBank accession numbers. The blue colour denotes percentage identity. The missing residues in the IVD-1 mutant identified in this work are indicated with stars. E) ACS-19 from *C. elegans* (CAA91274.1) was aligned with *Homo sapiens* ACSS2 (AAH98422.1), *Drosophila* ACS (AAF51695.2) and *S. cerevisiae* Acs1p (AAC04979.1). In brackets are the GenBank accession numbers. Blue color denotes the percentage identity. The mutation site in *C. elegans* ACS-19 identified in this work is indicated by a star.

Supplemental Figure 2

Chromosomal rescue of *ivd-1(hh6)* and *acs-19(hh5).* A) *ivd-1(hh6)* mutants without or after extrachromosomal expression of the *ivd-1* gene present on the fosmid

WRM061bH04 (*ivd-1(hh6)+ivd-1*). After injection of the fosmid 60.1% (+/- 28.4 s.d, n=38, 4 independently injected lines) of the worms carrying the extrachromosomal array showed no GFP fluorescence, indicating suppression of the Ub-GFP stabilization, as compared to 3.5% (+/-1.1 s.d, n=327,** $p \leq 0.01$) of the worms that did not carry the array. B) *acs-19(hh5)* mutants without (*acs-19(hh5*)) or after chromosomal expression of the *acs-19* gene present on fosmid WRM0620aH08 (*acs-19(hh5) +acs-19*). After fosmid injection 57.0% (+/-9.3 s.d, n=279, 2 independently injected lines) of the worms carrying the extrachromosomal array showed no GFP expression whereas 19.1% (+/- 8.0 s.d, *** $p \leq 0.001$) not carrying the array were GFP-negative. C) *acs-19(hh5)* mutants without (*acs-19 (-)*) or after chromosomal expression of the *acs-19* gene present on fosmid WRM0620aH08 (*acs-19(+)* were analyzed at day one of adulthood. Injection 1 and 2 denote two independent strains obtained after injection. Worms were collected in SDS sample buffer and extracts analyzed by western blotting against GFP and tubulin. D) Worms expressing ^{K29,48R}-Ub-GFP or GFP were depleted by RNAi for the indicated genes and analyzed by western blotting against GFP and tubulin. E) Fluorescence and Nomarski images of day 1 adult worms expressing UbV-GFP treated with RNAi against the *C. elegans* orthologs of human Branched chain keto acid dehydrogenase E1 (*tag173*) and alpha methylcrotonyl coenzyme A carboxylase 1 (*mccc-1*) involved in leucine catabolism.

Supplemental Figure 3

Stress response and protein turnover after RNAi. A) RNAi-treated hermaphrodites were analyzed for the expression of *hsp-4::GFP* at day 1 adulthood. Western blot of lysates

were probed against GFP and tubulin. B) Worms expressing *hsp-70::GFP* were treated with RNAi till day 1 of adulthood at 20°C or on NGM seeded with OP50 at 20°C (control 20°C). For heat shock day 1 old worms were placed at 35°C for 30 min and allowed to recover at 20°C for 4 hr. Extracts of worms were analyzed by western blotting as in (A). C) RNAi-treated hermaphrodites were analyzed for the expression of *hsp-6::GFP* at day 1 adulthood as in (A). D) ROS levels of the indicated strains were measured in day 1 adult hermaphrodites. Data display averages of 3 to 4 independent experiments +/- s.e.m., ***p ≤ 0.001. E) Worm development on control or 2 □M antimycin A-containing plates. A (Adults), L (Larvae), data display the averages of three experiments +/- s.d., *p ≤ 0.05, **p ≤ 0.01.

Supplemental Figure 4

Analysis of tissue culture and patient cells. A) MelJuSo cell lines stably expressing UbR-YFP were pre-treated for 18 hours with ethanol as control (-) or 100 □M antimycin A (in ethanol) followed by 100 □g/ml cycloheximide for the indicated time points. Cell lysates were analyzed by western blotting against YFP as shown in Figure 6, but. a strong exposure is presented to highlight the polyubiquitylated substrate. B) Similar to (A) but MelJuSo cells stably expressing UbG76V-YFP from Figure 6 A are displayed. C) Primary human control fibroblasts (c), and fibroblasts from IVD-deficient patients with severe (c.IVS4+2T>C) or mild phenotypes (c932C>T) were examined for the levels of IVD by western blotting. D) Lysates of cell lines from (C) were analyzed by western blotting against ubiquitin and tubulin. E) Cybrid cells containing the G6930A mutation in the *COX1* gene (G6930A) (Bruno et al., 1999) compared to the corresponding wild-type cells (WT) were transfected with UbR-GFP and mCherry as transfection control. Cell

lysates were analyzed by western blotting against GFP, mCherry, and tubulin. F) same as (E), but cells were transfected with UbG76V-GFP. We observed an accumulation of a cleavage product (indicated by a star), similar to the cleavage product reported previously for tissue culture cells after proteasomal inhibition (Dantuma et al., 2000). This seems to reflect increased hydrolytic processing of the stabilized UbG76V-GFP in these cells.

Supplemental Figure 5

Cellular surveillance in *ivd-1(hh6), acs-19(hh5)* and *hecd-1(tm2371)* mutants.

A) Wild type (WT) or mutant hermaphrodites expressing *sur-5::UbV-GFP* were treated with *control* or *cdc-48(RNAi)* as indicated and analyzed by fluorescence microscopy. Scale bar: 1 mm. B) Lysates of worms shown in panel (A) were examined by western blotting with anti-GFP and anti-tubulin antibodies. C) Lifespan analysis of worms as indicated grown from L1 stage at 20°C on NGM or NGM containing 10 mM N-acetylcysteine (NAC) seeded with OP50. Detailed statistics are provided in Table S5.

Bruno, C., Martinuzzi, A., Tang, Y., Andreu, A.L., Pallotti, F., Bonilla, E., Shanske, S., Fu, J., Sue, C.M., Angelini, C*., et al.* (1999). A stop-codon mutation in the human mtDNA cytochrome c oxidase I gene disrupts the functional structure of complex IV. Am J Hum Genet *65*, 611-620.

Dantuma, N.P., Lindsten, K., Glas, R., Jellne, M., and Masucci, M.G. (2000). Short-lived green fluorescent proteins for quantifying ubiquitin/proteasome-dependent proteolysis in living cells. Nat Biotechnol *18*, 538-543.

Davis, M.W., Hammarlund, M., Harrach, T., Hullett, P., Olsen, S., and Jorgensen, E.M. (2005). Rapid single nucleotide polymorphism mapping in C. elegans. BMC Genomics *6*, 118.

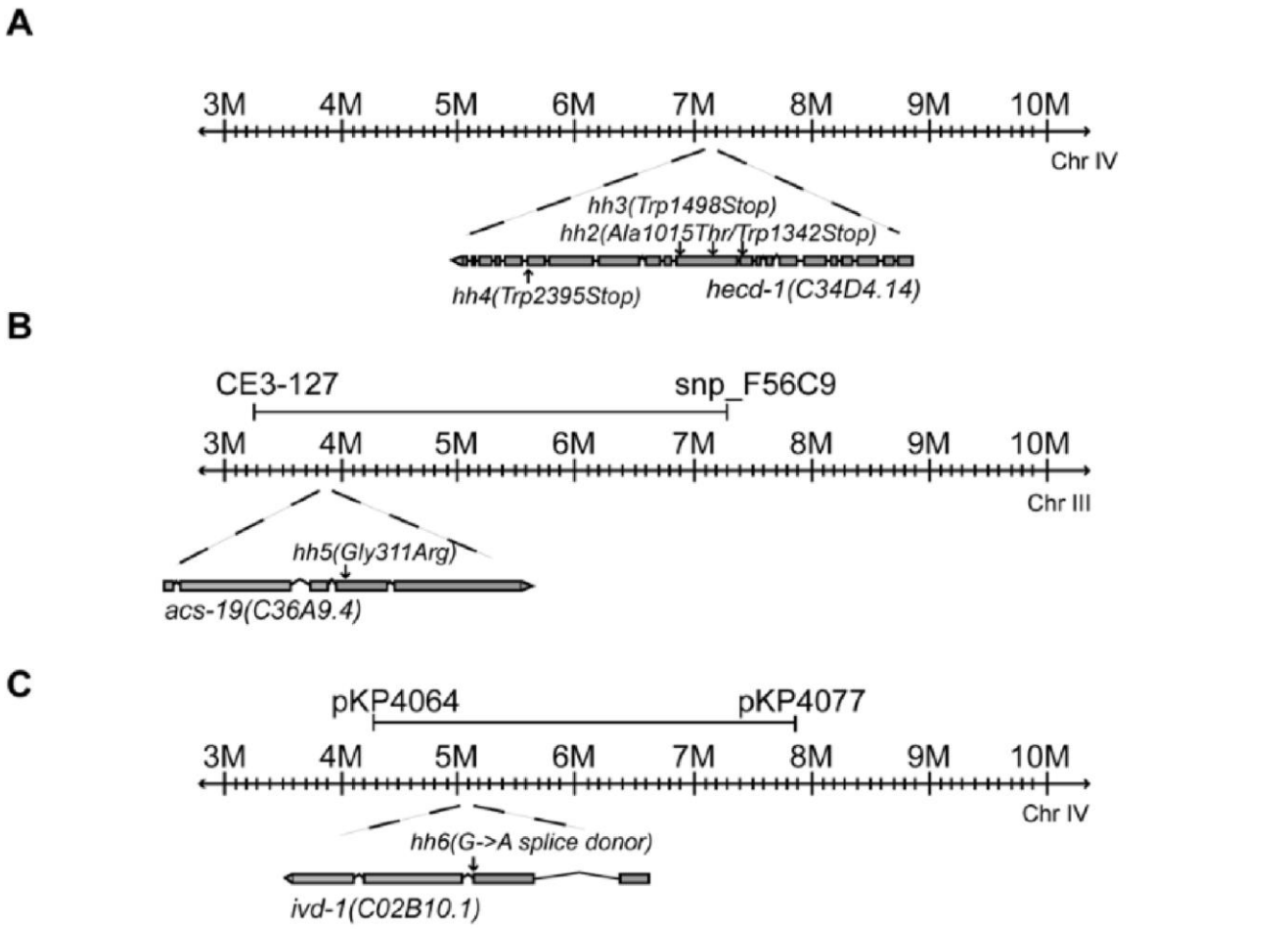

D

```
                                                                                                  * * * * * * *
Drosophila      94 DFGGTGGSYLDHCIIMEEFSRAAGGVALSYGAHSNLCINQLTKNGTPE 141
C. elegans      94 EYGGSGMNYFSHVIAMEELSRAAGGIALSYGAHSNLCINQIVRNGSEE 141
Homo sapiens    97 QYGGSGLGYLEHVLVMEEISRASGAVGLSYGAHSNLCINQLVRNGNEA 144
Arabidopsis     86 EYGGLGLGYLYHCIAMEEISRASGSVALSYGAHSNLCINQLVRNGTAA 133

Drosophila     142 QKEKYLPKLCSGEHVGGLAMSEPGAGSDVVSMKLRAERKGDYYVLNGS 189
C. elegans     142 QRKKYLPKLISGEHMGALAMSEAQAGSDVVSMKLRAEKKGDKYVLNGT 189
Homo sapiens   145 QKEKYLPKLISGEYIGALAMSEPNAGSDVVSMKLKAEKKGNHYILNGN 192
Arabidopsis    134 QKEKYLPKLISGEHVGALAMSEPNAGSDVVGMKCKAEKVDGGYILNGN 181
                   * * * * * * * *
```

E

```
                                                  *
Homo sapiens   209 WCDAEDPLFILYTSGSTGKPKGVVHTVGGYMLYVATTFKYVFDFHAED 256
Drosophila     273 WMDAEDPLFMLYTSGSTGKPKGVLHTTAGYLLYAATTFKIVFDYKPGD 320
C. elegans     283 WMDSEDPLFILYTSGSTGKPKGIQHTTAGYMTYAYATTKYTFDAQEDD 330
S. cerevisiae  308 PVDSEDPLFLLYTSGSTGAPKGVQHSTAGYLLGALLTMRYTFDTHQED 355
```

Supplemental Figure 2

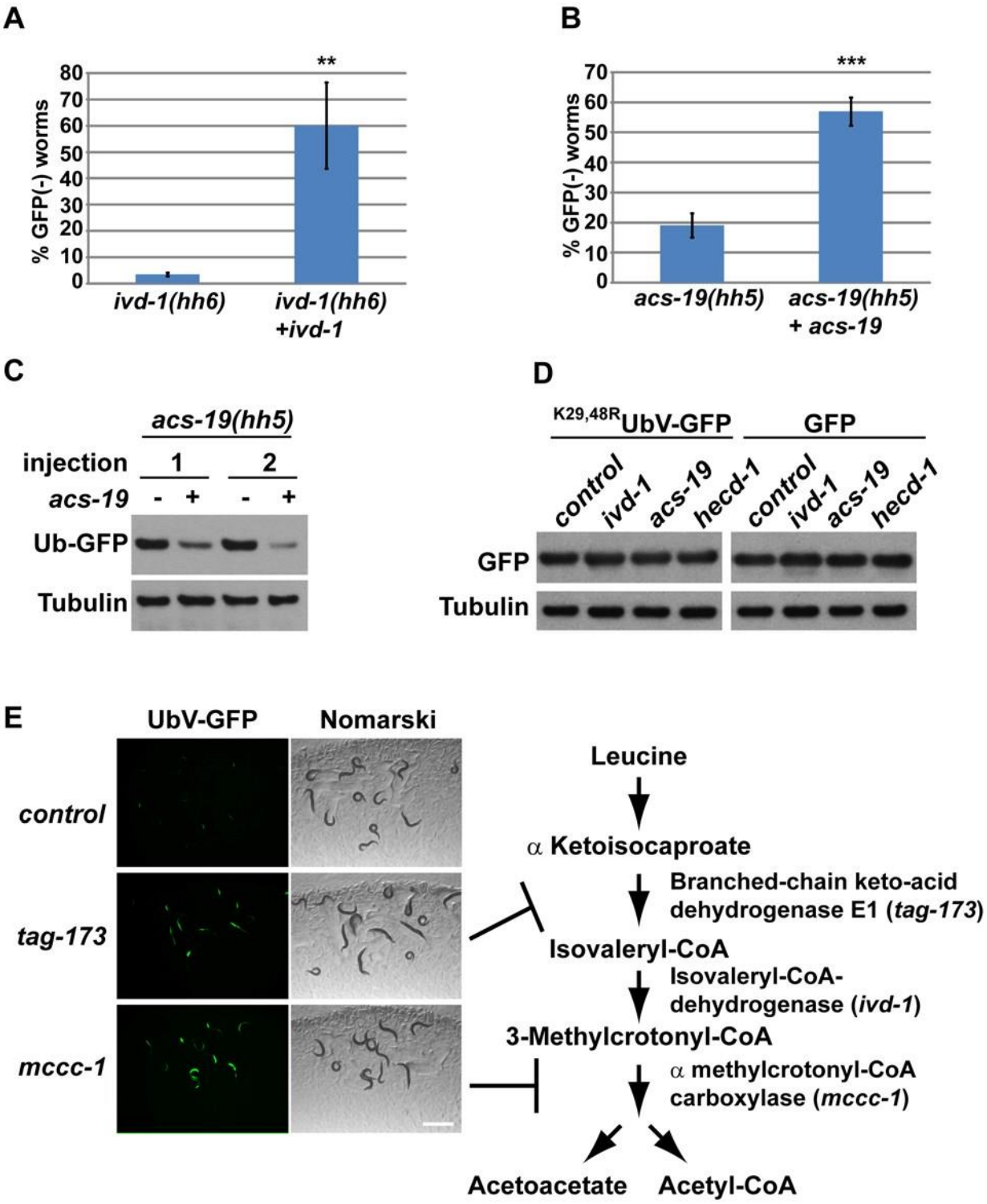

Supplemental Figure 2

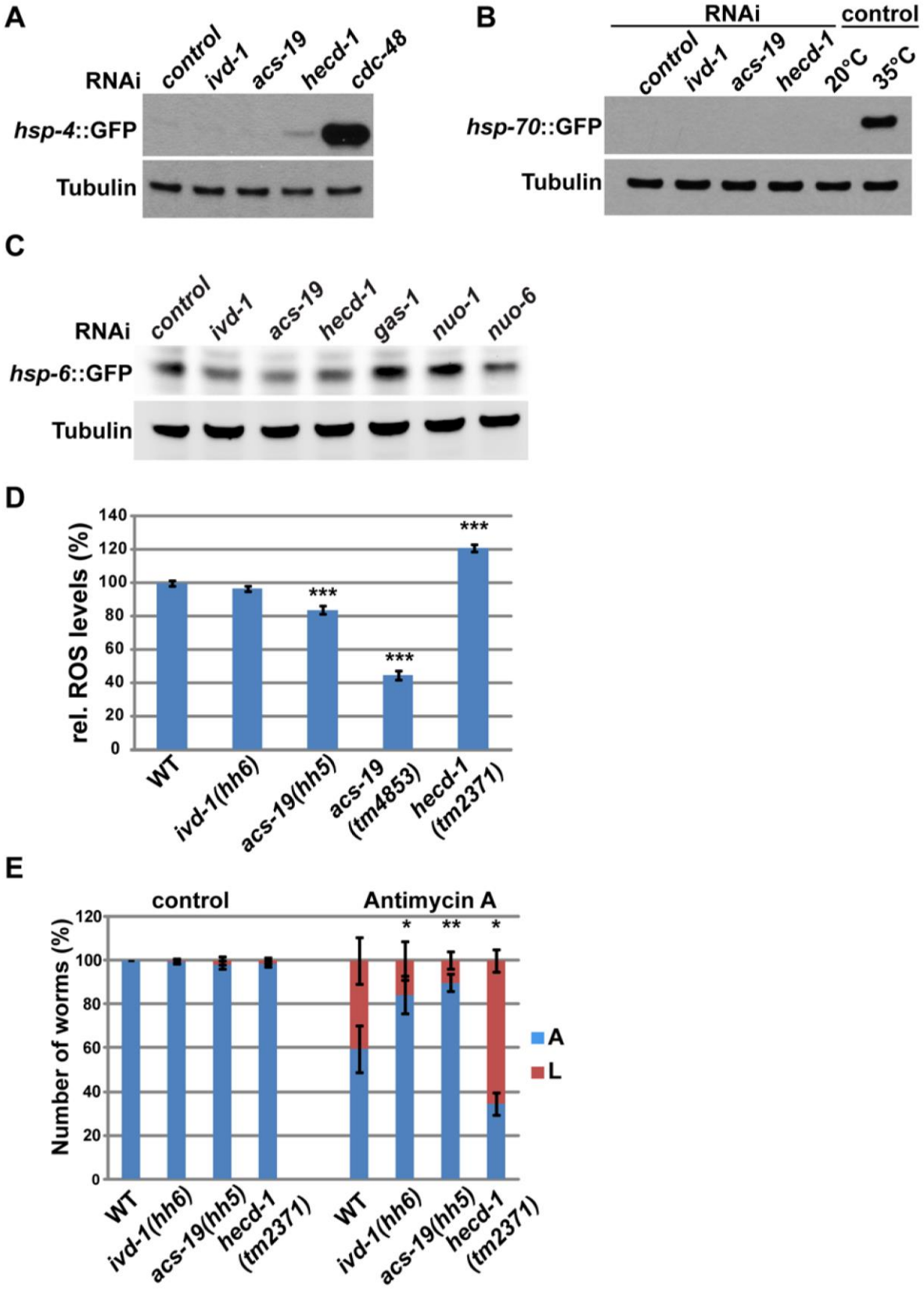

Supplemental Figure 3

Supplemental Figure 4

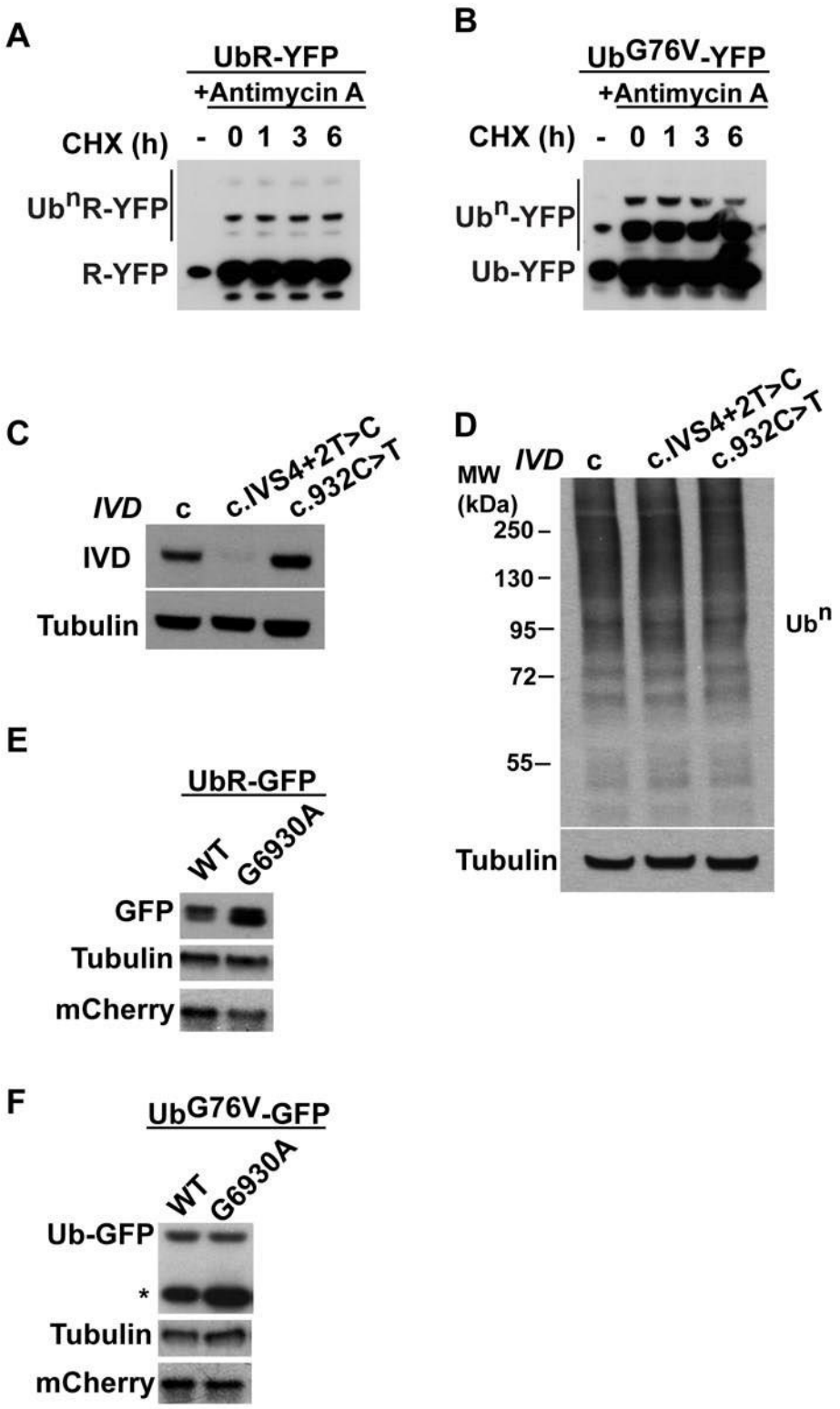

Supplemental Figure 4

Supplemental Figure 5

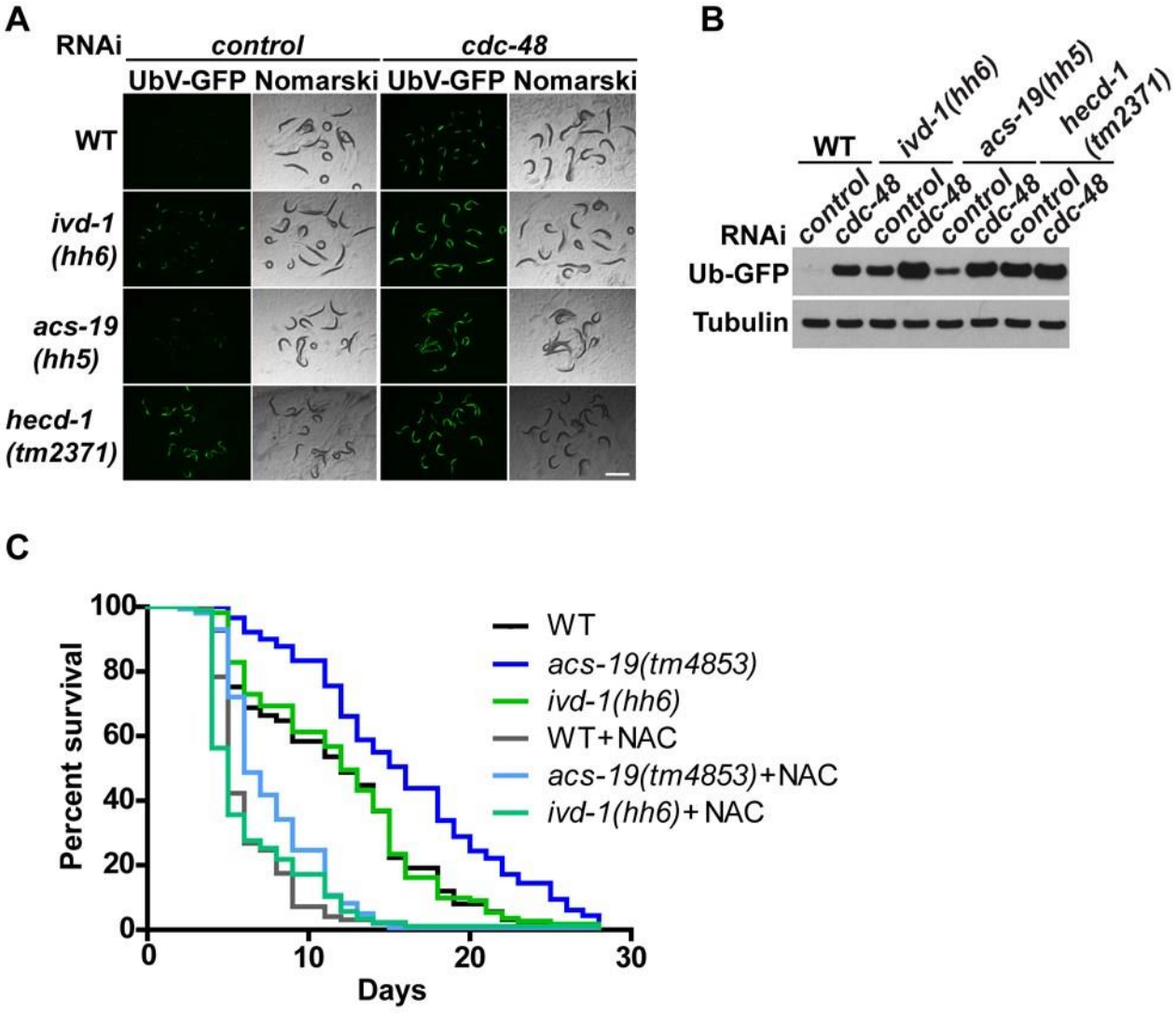

Supplemental Figure 5

Mutant	Development		Tissue			
	L	A	P	I	V	T
hecd-1 (hh2)	+	+	+	+	+	+
hecd-1 (hh3)	+	+	+	+	+	+
hecd-1 (hh4)	+	+	+	+	+	+
acs-19 (hh5)	+	+	-	+	-	-
ivd-1 (hh6)	+	+	-	+	-	-
hecd-1 (hh9)	+	+	+	+	+	+

Table S1. Stabilisation of Ub-GFP in mutants identified. L: during larval stage, A: during adult stage, P: pharynx, I: intestine, V: vulva, T: tail.

Supplemental Table 2

Mutants	*hecd-1 (hh2)*	*hecd-1 (hh3)*	*hecd-1 (hh4)*	*ivd-1 (hh6)*	*hecd-1 (hh9)*	*acs-19 (hh5)*
hecd-1(hh2)		-	-	+	-	
hecd-1(hh3)			-	+	-	
hecd-1(hh4)				+	-	
hecd-1(tm2371)	-	-		+		
ivd-1(hh6)					+	
acs-19(tm4853)						-
eel-1(ok1575)				+		
ubc-1(gk14)				+		
uba-1(it129)				+		

Table S2. Non-complementation tests to assign mutant complementation groups. Plus (+): mutants are complementing each other, minus(-): mutants are non-complementing.

Primary human fibroblasts	***IVD* gene mutations**	**Metabolite accumulation**		**Clinical presentation**
		Blood isovalerylcarnitine	**Urine isovalerylglycine**	
IVA severe	c.IVS4+2T>C/ c.IVS4+2T>C	15 µM	1400 mmol/mol creatinine	Diagnosed during neonatal metabolic crisis, learning disability
IVA mild	c.932C>T (p.A282V)/ c.932C>T (p.A282V)	1.4 µM	30 mmol/mol creatinine	Diagnosed by metabolic newborn screening, asymptomatic

Table S3. Cellular genotype, metabolite pattern and clinical phenotype of individuals with severe and mild isovaleric acidemia. IVA: isovaleric acidemia, IVD: isovalerylCoA dehydrogenase.

Supplemental Table 5

Experiment 1	mean	Stdv	n	SEM	p-value (t-test)	p-value (Mantel-Cox)
WT	13.45	6.8	33	1.2		
acs-19(hh5)	14.44	9.1	36	1.5	WT 0.394 *acs-19(tm4853)* 0.125	0.214 0.624
acs-19(tm4853)	17.87	6.6	47	1.0	WT < 0.01	<0.05
ivd-1(hh6)	14.2	6.7	35	1.1	WT 0.911	0.635
					acs-19(hh5) 0.68	0.290
					acs-19(tm4853) <0.01	<0.05
Experiment 2						
WT	12.89	6.6	36	1.1		
acs-19(hh5)	16.12	7.9	33	1.4	WT <0.001 *acs-19(tm4853)* <0.001	<0.05 0.830
acs-19(tm4853)	16.68	6.3	44	0.9	WT <0.001	<0.05
ivd-1(hh6)	16.48	7.5	29	1.4	WT <0.001	<0.05
					acs-19(hh5) <0.001	0.824
					acs-19(tm4853) <0.001	0.703
Experiment 3						
WT	13.73	7.7	30	1.4		
acs-19(hh5)	18.78	7.0	36	1.2	WT <0.001 *acs-19(tm4853)* < 0.001	<0.05 0.055
acs-19(tm4853)	15.62	7.3	42	1.1	WT <0.01	0.499
ivd-1(hh6)	14.76	7.8	37	1.3	WT <0.001	0.611
					acs-19(hh5) <0.001	0.110
					acs-19(tm4853) 0.206	0.905
Experiment 4						
WT	13.51	6.6	37	1.1		
acs-19(hh5)	16.98	6.8	42	1.1	WT <0.001 *acs-19(tm4853)* 0.07	<0.05 0.536
acs-19(tm4853)	17.26	7.7	46	1.1	WT <0.001	<0.01
ivd-1(hh6)	15.43	7.2	40	1.1	WT <0.001	0.139
					acs-19(hh5) <0.001	0.452
					acs-19(tm4853) 0.11	0.215
All combined						
WT	13.38	6.8	136	0.6		
acs-19(hh5)	16.61	7.8	147	0.6	WT <0.001 *acs-19(tm4853)* 0.724	<0.001 0.528
acs-19(tm4853)	16.89	7.0	179	0.5	WT <0.001	<0.001
ivd-1(hh6)	15.16	7.3	141	0.6	WT 0.036	<0.05
					acs-19(hh5) 0.066	0.067
					acs-19(tm4853) 0.344	0.123

Table S4 Statistical analysis of wild-type (WT), *ivd-1(hh6), acs-19(hh5)* and *acs-19(tm4853)* grown on OP50. n= number of animals.

Experiment 1	mean	Stdv	n	SEM	p-value (t-test)	p-value (Mantel-Cox)
WT	12.42	5.7	31	1.0		
acs-19(tm4853)	16.11	6.1	45	0.9	WT 0.222 *ivd-1(hh5)* 0.294	<0.01 <0.05
ivd-1(hh6)	12.03	5.7	29	1.1	WT 0.170	0.856
WT + NAC	6.17	1.8	24	0.4	WT <0.001	<0.001
***acs-19(tm4853)*+ NAC**	7.92	3.0	38	0.5	WT <0.001 WT + NAC 0.166 *acs-19(tm4853)* <0.001	<0.001 <0.01 <0.001
***ivd-1(hh6)*+ NAC**	5.47	2.6	17	0.6	WT <0.001 WT + NAC 0.509 *ivd-1(hh6)* <0.001	<0.001 0.307 <0.001
Experiment 2						
WT	10.97	5.9	32	1.1		
acs-19(tm4853)	15.61	6.0	44	0.9	WT <0.001 *ivd-1(hh5)* <0.001	<0.01 <0.01
ivd-1(hh6)	11.06	5.1	31	0.9	WT <0.01	0.917
WT + NAC	6.49	2.6	23	0.5	WT <0.01	<0.01
***acs-19(tm4853)*+ NAC**	7.19	2.6	42	0.4	WT <0.001 WT + NAC <0.05 *acs-19(tm4853)* <0.001	<0.001 0.339 <0.001
***ivd-1(hh6)*+ NAC**	6.43	3.0	21	0.7	WT <0.001 WT + NAC 0.131 *ivd-1(hh6)* <0.001	<0.001 0.798 <0.001
Experiment 3						
WT	11.51	5.4	35	0.9		
acs-19(tm4853)	16.19	6.8	42	1.0	WT <0.001 *ivd-1(hh5)* <0.01	<0.001 0.101
ivd-1(hh6)	13.00	6.3	24	1.3	WT <0.001	0.305
WT + NAC	6.00	3.2	25	0.6	WT <0.001	<0.001
***acs-19(tm4853)*+ NAC**	7.46	2.8	37	0.5	WT <0.001 WT + NAC 0.798 *acs-19(tm4853)* <0.001	<0.001 0.068 <0.001
***ivd-1(hh6)*+ NAC**	7.08	5.3	25	1.1	WT <0.01 WT + NAC 0.064 *ivd-1(hh6)* <0.001	<0.01 0.712 <0.001
Experiment 4						
WT	12.07	6.4	27	1.2		
acs-19(tm4853)	16.18	6.4	49	0.9	WT 0.278 *ivd-1(hh5)* 0.068	<0.05 <0.05
ivd-1(hh6)	12.37	5.6	27	1.1	WT 0.362	0.975
WT + NAC	6.08	2.3	25	0.5	WT <0.001	<0.001
***acs-19(tm4853)*+ NAC**	8.27	4.5	41	0.7	WT <0.001 WT + NAC 0.050 *acs-19(tm4853)* <0.001	<0.01 <0.01 <0.001

Supplemental Table 7

All combined						
WT	11.72	5.8	125	0.5		
acs-19(tm4853)	16.03	6.3	180	0.5	WT <0.001 *ivd-1(hh5)* <0.001	<0.001 <0.001
ivd-1(hh6)	12.05	5.6	111	0.5	WT 0.120	0.715
WT + NAC	6.18	2.5	97	0.3	WT <0.001	<0.001
***acs-19(tm4853)*+ NAC**	7.71	3.3	158	0.3	WT <0.001 WT + NAC 0.05 *acs-19(tm4853)* <0.001	<0.001 <0.001 <0.001
***ivd-1(hh6)*+ NAC**	6.38	3.8	87	0.4	WT <0.001 WT + NAC 0.39 *ivd-1(hh6)* <0.001	<0.001 <0.001 0.964 <0.001
***ivd-1(hh6)*+ NAC**	6.25	3.4	24	0.7	WT <0.001 WT + NAC 0.233 *ivd-1(hh6)* <0.001	<0.001 0.861 <0.001

Table S5 Statistical analysis of wild-type (WT), *ivd-1(hh6),* and *acs-19(tm4853)* mutants on NGM plates or NGM plates containing 10 mM NAC (+NAC) seeded with OP50. n= number of animals.